DEFORMATION AND FINITE SIZE EFFECTS IN COOPERATIVE MOLECULAR MOTORS

A THESIS
SUBMITTED TO THE DEPARTMENT OF PHYSICS
AND THE INSTITUTE OF ENGINEERING AND SCIENCES
OF BİLKENT UNIVERSITY
IN PARTIAL FULFILLMENT OF THE REQUIREMENTS
FOR THE DEGREE OF DOCTOR OF PHILOSOPHY

By

Sencer Taneri

July 2002

I certify that I have read this thesis and that in my opinion it is fully adequate, in scope and in quality, as a dissertation for the degree of Doctor of Philosophy.

Prof. Dr. M. Cemal Yalabık (Supervisor)

I certify that I have read this thesis and that in my opinion it is fully adequate, in scope and in quality, as a dissertation for the degree of Doctor of Philosophy.

Prof. Bilal Tanatar

I certify that I have read this thesis and that in my opinion it is fully adequate, in scope and in quality, as a dissertation for the degree of Doctor of Philosophy.

Prof. Atilla Erçelebi

I certify that I have read this thesis and that in my opinion it is fully adequate, in scope and in quality, as a dissertation for the degree of Doctor of Philosophy.

Prof. Şinasi Ellialtıoğlu

I certify that I have read this thesis and that in my opinion it is fully adequate, in scope and in quality, as a dissertation for the degree of Doctor of Philosophy.

Prof. Şefik Süzer

Approved for the Institute of Engineering and Science:

Prof. Mehmet Baray,
Director of Institute of Engineering and Science

Abstract

DEFORMATION AND FINITE SIZE EFFECTS IN COOPERATIVE MOLECULAR MOTORS

Sencer Taneri
Doctor of Philosophy in Physics
Supervisor: Prof. Dr. M. Cemal Yalabık
July 2002

Motor protein systems have been of considerable interest lately. In these studies muscle contraction is modeled as the sliding of two filaments made of protein particles over one another, that is the sliding of the backbone filament on the track filament. In order to make the analytical analysis easy these filaments are assumed to be of infinite length or mass. This enables the understanding of the sliding of motility assays with constant velocity and generation of constant force. However, finite size in length and mass brings fluctuations in velocity around certain values, and changes in direction through intermittent transitions. It is possible to associate time constants to this kind of behavior. It turns out that the magnitude of the time constant being created during the process is proportional to both the length of the filament and the mass of the protein particles.

Deformation phenomenon stems from internally generated forces which so far has been examined as axonemal deformations. The elastic coupling of the protein particles to the backbone has been studied separately, which in fact

is also related to the generation of internal forces. Instead of focusing on the axonemal deformations, we implemented an Ising-like potential contribution to our computation to study the elastic coupling which makes the computation easier. We found out that for certain range of parameters that measures the deformation strength, one attains a better motor because of more intense force generation at the expanse of getting a lower sliding velocity.

Özet

MOLEKÜLER MOTORLARDA DEFORMASYON VE SONLU UZUNLUK ETKİLERİ

Sencer Taneri
Fizik Doktora
Tez Yöneticisi: Prof. Dr. M. Cemal Yalabık
Temmuz 2002

Motor protein sistemleri son zamanlarda büyük ilgi toplamıştır. Bu çalışmalarda kas kasılması, protein parçacıklarından yapılmış omurga ve ray filamanlarının biribiri üzerinde kaymasıyla modellenmiştir. Analitik analizi kolaylaştırmak için bu filamanların sonsuz uzunluk ve kütleden oluştukları kabul edilmektedir. Bu sabit hız ve sabit kuvvet üretimiyle hareket eden sistemin anlaşılmasını kolaylaştırmaktadır. Yalnız, uzunlukta ve kütledeki sonluluk hızın belli bir değer çevresinde değişmesine sebep olur ki bu geçişme sırasında bu değerin işaret değiştirmesine de sebep olur. Bu davranış şekline iyi bilinen Arrhenius Kanunu sayesinde bir zaman sabiti tanımlamak mümkündür. Meydana çıkan enerji bariyerinin büyüklüğünün filamanın uzunluğu ve protein parçacıklarının kütlelerinin büyüklüğüyle orantılı olduğu ortaya çıkmaktadır.

Deformasyon fenomeni şimdiye değin kesitsel deformasyonlar olarak incelenmiş iç kuvvetlerin üretilmesiyle ortaya çıkar. Protein parçacıklarının omurgaya elastik bağlanması ayrıca kuvvet üretimi ile ilgilidir. Kesitsel

deformasyonlara odaklanmak yerine, hesaplamaya elastik bağlılığı, hesaplamayı daha kolay kılmak için bir Ising benzeri potansiyeli katarak çalıştık. Deformasyon büyüklüğünü ölçen parametrelerin bazıları için düşük kayma hızlarina karşın daha fazla kuvvet üretilmesiyle daha iyi bir motor elde edildiğini saptadık.

Anahtar sözcükler:

Moleküler Motorlar, Deformasyon, Sonlu Boyut Etkisi .

Acknowledgement

It is my pleasure to express gratitude to my supervisor, Dr. M. Cemal Yalabık, for his guidance and support throughout my graduate study, and the development of the present study in particular.

I would like to thank to my old friends Ty Buxman, Bill Talbert, Matthew Crocket, Alexander, Vilademir from USC together with Tuğrul Senger, Özgür Özer, Kaan Güven, Özgür Cakır and Dr. Soner Yıldırım, and commemorate Justin', Dr.Gene Bickers, Dr.Gail Walenga, late Dr.Judith Grayson again from USC and Dr.Salim Cıracı who have inspired me for research before I started the Ph.D program.

I would like to thank to Alper Dizdar and Burak Gökmen for their moral and spiritual support.

I would like to thank Dr.Bilal Tanatar, Dr.Atilla Erçelebi, Dr.Atilla Aydınlı, Dr. Zafer Gedık and Emine Benderlioglu for their moral and technical support, in every case that I needed some.

I also thank to Dr. Andrzej Cieplak and Dr. Şefik Süzer for fruitful discussions.

I also like to thank to Dr. Ordal Demokan from METU for his tutorial in International Physics Olympiads which prepared me for study in this field of

Science.

I also thank to Şinasi Ellialtıoğlu for bothering to come from METU for jury membership.

I also want to notify and feel grateful for the honorable Dr.Igor Kulik for his attitude in Fall 1997 class.

Finally, I express my love and gratitude to my dear parents Ipek and Neylan Taneri who have always encouraged and supported me by all means.

Contents

List of Figures

List of Tables

Chapter 1

INTRODUCTION

Molecular motors are bio-chemical systems, which consist of two filaments sliding on one another. The energetics of these proteins result in a net relative force between the filaments, which may lead to sustained motion. A collection of molecular motors acting cooperatively as a system, also appears in many biological systems, and is responsible, for example for muscle contraction. The theoretical analysis of such cooperating systems requires simulation techniques, which are used in the field of non-equilibrium statistical physics such as Monte-Carlo and Langevin equation, due to complexity involved in the mechanics. We have in particular studied the effects of elastic coupling among motors, which form a linear chain, and effect the finite size of the systems. This latter analysis is significant because, to our knowledge all other work in the problem assumes infinite system sizes to simplify the mathematics (see for example Reference 1).

This thesis describes deformation and finite size effect aspects of cooperative molecular motors operation.

We will start with a general description of the biological system to motivate the mathematical model, which we will be using. The filaments that are made of molecular motors may serve as track filaments or as trail filaments.

Track filaments are typically classified into several families as myosin, kinesin or dynein. Myosin always slides on actin while kinesin and dynein always slide on microtubles. A schematic illustration of these two types of phenomena is given below.[1]

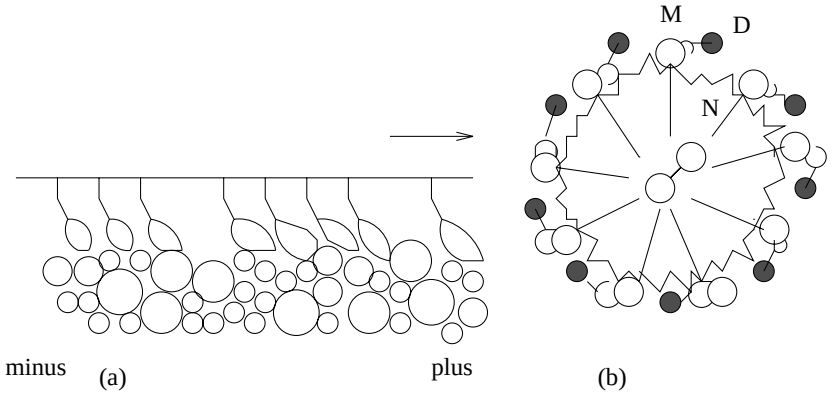

Figure 1.1: (a)Myosin interacting with actin filaments.(b) Microtubles (M) are arranged in a cylindrical fashion. Dynein motors(D) are attached to microtuble doublets. Elastic elements (N) are nexin indicated as springs, see F.Jülicher, Ref[1].

One should note that dynein and kinesin move in opposite directions in a composite material. Myosin occurs with in normal cells where they play the important role of cell motility and organization of actin. Kinesin occurs vastly in neurons playing the role in transport of vesicles along the axon towards the synapse. The head of both types of trail filaments are of size about 10-20 nm and are responsible for the elementary force generation. The tails are used to attach the motor to another structure, which usually serve as the elastic coupling to the environment, which can be used as a model to explain the oscillations occurring

in the muscles of some insects. The energy source of the sliding process is the hydrolysis reaction ATP$\longrightarrow$ ADP+P of ATP (Adenosine-triphosphate) to ADP and Phosphate (P). The motor protein M undergoes a chemical cycle binding ATP and hydrolizing the bound ATP. So, one can denote the different chemical states as M, M-ATP, M-ADP-P and M-ADP, see Fig 1.2.[1]

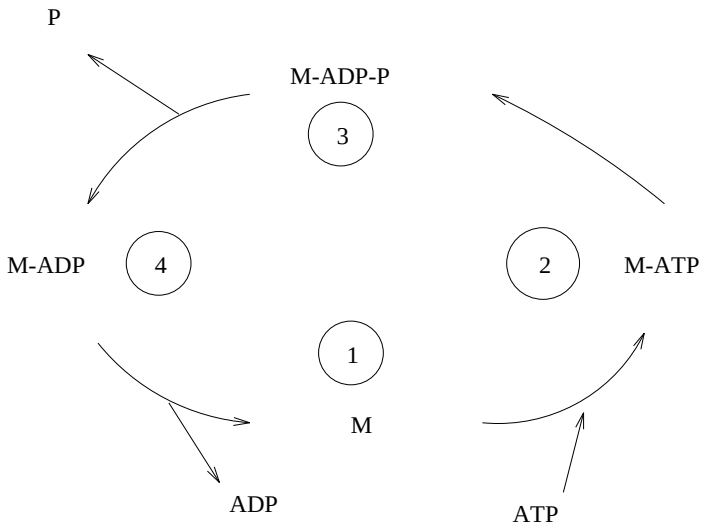

Figure 1.2: Chemical cycle of a motor molecule M. After the completion of one cycle the motor is unchanged but one ATP is hydrolyzed, see F. Jülicher, Ref[1].

As a result, the motor protein undergoes chemistry-driven changes between strongly or weakly bounded states ("attachments" and "detachments"), which create the motion along track filament. The force and motion generation of motor proteins can also be studied experimentally. The attachment of motors to a substrate (so called motility assays), results in the binding of the filaments in solution to the motors, and in the presence of ATP they start moving along the surface. Many filaments interact with a single filament and processivity becomes important in the observation of forces generated by the individual motor. Processivity denotes the proper proportionality constant of the transition rates,

which determines an observable force generation. For instance, myosin is not processive since it detaches from the filament during a significant period of time during which it can easily diffuse away from the filament. So different techniques must be used, see Fig 1.3.[1]

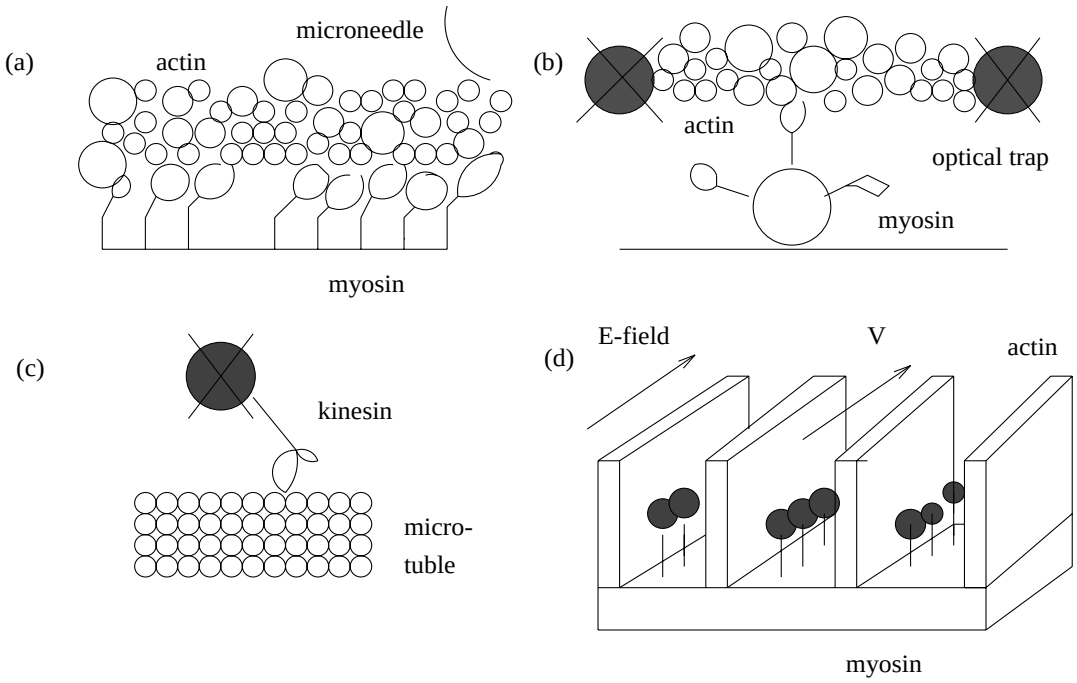

Figure 1.3: (a) Force generation by the deflection of a micro-needle. (b) Force measurement by optical traps. (c) Force generation observed by displacement of a bead in an optical trap. (d) Force induced by an electric field E in a motility assay using linear groves to orient the filament, see F.Jülicher, Ref[1].

Micron sized beads, which have been coated with low density motors and optical traps are used to bring the filament in contact with a bead and possibly only a single motor. Forces are then measured by observing the displacement in the trap or by fixing the actin and manipulating the bead with an optical trap. Such experiments reveal that the motor induces displacements of the order 5-10nm, which lasts for several milliseconds and peak forces of the order of 1 pN. Kinesin being processive can be observed with and without optical traps. The direct observation involves marking of the molecule with a florecent

dye. Otherwise, observation studies the velocity of motion as a function of an applied force. It has been shown that kinesin moves in step-wise fashion with characteristic steps of 8nm size, which coincides with the period of binding sites. This information will be used in the theory part when we simplify the situation into the simple saw-tooth potential model. Here, the forces generated are about 5pN.

Fluctuations play an important role for the functioning of the molecular motors since motion is generated along a one-dimensional polar and periodic structure. These fluctuations may be of both thermal origin or due to the stochasticity of individual molecule or chemical reactions. Therefore, concepts of non-equilibrium statistical physics comes into play. There is also the concept of artificially designed molecular motors suggesting that the physics of these systems is relevant for micro and nano-technical devices.

In the next chapter, we provide a background to related work done by other workers. Chapter 3 and Chapter 4 present our contributions to the field. The thesis is concluded in the final chapter.

Chapter 2

BACKGROUND

Two different facets of molecular motors were our targets of research: 1-Deformation and 2-Finite Size Effects. The second never been investigated before, was of special interest to us. On the other hand, our work on the first topic resulted in a publication.[2] In this section we provide a review of the work similar to the ones we have used, that had been carried out earlier, and that had formed the foundation of our work.

Several aspects of the cooperative molecular motor structure has been quite a fruitful topic for French scientists, pioneered by Frank Jülicher. Some of these aspects are, the ATP concentration dependence of the external load for various ATP concentrations, and the efficiency of the motor as a function of the external force load.

We will first discuss the simple models involved in cooperative molecular motor systems in order to analyze the sliding process at the molecular scale. The simplest model involves rigid coupling where the molecular motor system is assumed as a collection of an infinite number of particles. Here, each particle is a molecular motor and the collection defines the trail filament, which slides on the track filament. These filaments are each assigned an energy level between which

the particles are free to shift sides. However, these energy levels have different configurations, one being constant and the other being periodic; see Fig 2.1.[1]

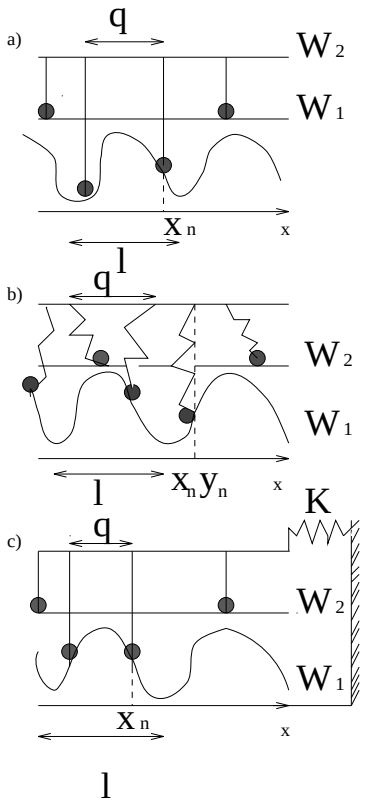

Figure 2.1: (a) Rigid coupling. (b) Elastic coupling to rigid backbone. (c) Elastic coupling to environment, see F.Jülicher, Ref[1].

The particles are said to be excited when they are detached from the upper constant energy level to the lower periodic potential level, which happens at certain transition frequencies determined via a weighting factor depending on the energy difference and temperature. The ATP concentration on the saw-tooth potential present at certain parts of the track also triggers transitions. The detachment process determines the force acting on the particles and thus on the trailer so that we end up with the collective motor properties. We will now discuss how the transition frequency depends on the energy difference, temperature and

ATP concentration, see Fig 2.2.[1]

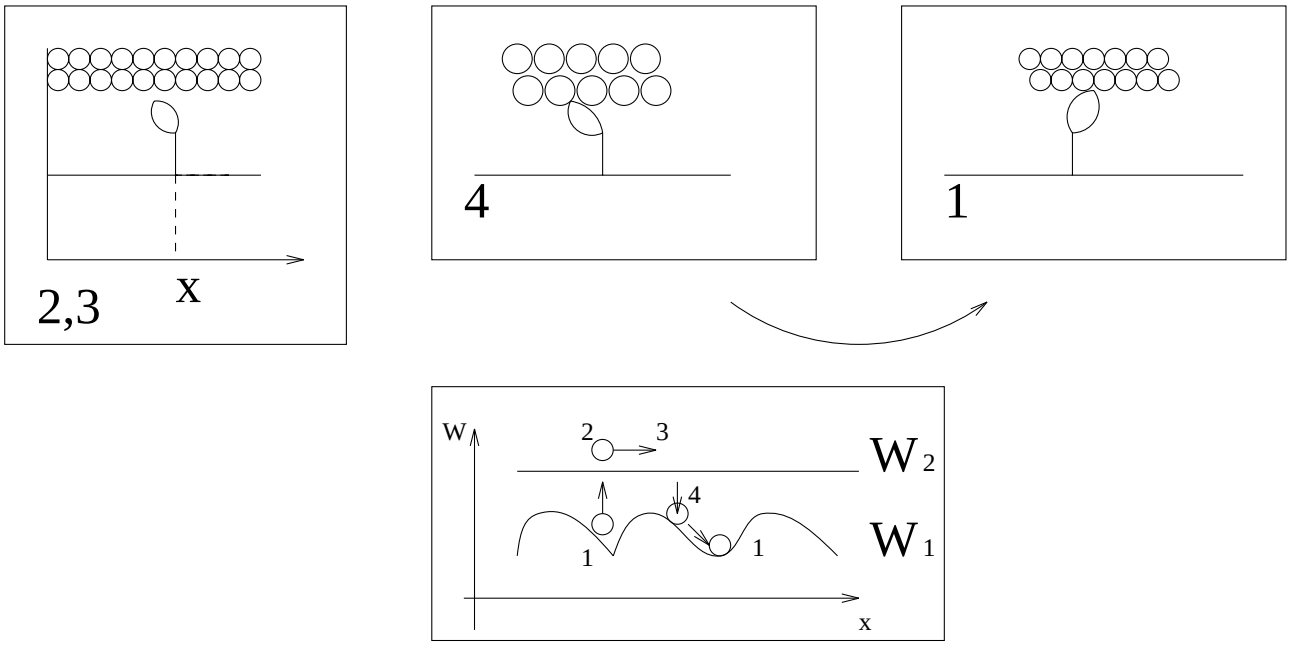

Figure 2.2: (1) Binding of an ATP molecule. (2) hydrolysis. (3) rebinding and generation of force. (4) displacement, see Frank Jülicher, Ref[1].

The chemical reaction cycle can be divided into two subsets as,

$$M + ATP \leftrightarrow \overset{\alpha_1}{\beta_1} M - ADP - P \tag{2.1}$$

$$M + ADP + P \leftrightarrow \overset{\alpha_2}{\beta_2} M - ADP - P \tag{2.2}$$

where α_1 and α_2 denote binding and hydrolysis coefficients and β_1 and β_2 denote rebinding and release coefficients as are depicted in Figure 2.2. For chemical energies, if $\Delta\mu = \mu_{ATP} - \mu_{ADP} - \mu_P$ then,

$$\alpha_1/\alpha_2 = \exp((W_1 - W_2 + \Delta\mu)/kT) \tag{2.3}$$

and,

$$\beta_1/\beta_2 = \exp((W_1 - W_2)/kT) \tag{2.4}$$

can be obtained from the construction of the detailed balance via Boltzmann equation with k being the Boltzmann constant and T the temperature. Then, distribution rates are simply superpositions as $\omega_i = \alpha_i + \beta_i$

$$\omega_1(x) = \alpha(x)\exp((W_1 + \Delta\mu)/kT) + \beta(x)\exp(W_1/kT) \quad (2.5)$$

$$\omega_2(x) = (\alpha(x) + \beta(x)))\exp(W_2/kT) \quad (2.6)$$

$$(2.7)$$

where $\alpha(x)$ and $\beta(x)$ are arbitrary functions. For $\Delta\mu = 0$,

$$\omega_1/\omega_2 = \exp((W_1 - W_2)/kT), \quad (2.8)$$

and for non-zero $\Delta\mu$,

$$\omega_1/\omega_2 = \exp((W_1 - W_2)/kT) + \Omega. \quad (2.9)$$

Here, Ω is called the excitation amplitude and depends on the ATP concentration in the form

$$\Omega \sim C_{ATP}/C_{ADP}C_P - \exp(\Delta\mu_o/kT), \quad (2.10)$$

where C stands for the various concentration fractions. The efficiency of the motor can be calculated by considering the work performed and chemical energy consumed in unit time as,

$$W = -F_{ext}V \quad (2.11)$$

$$Q = r\mu/\Delta t \quad (2.12)$$

if r is the number of chemical cycles performed per unit time. Thus, one gets the expression for the efficiency to be,

$$\eta = -F_{ext}V/r\mu \tag{2.13}$$

Choosing a potential amplitude $W_1(0.5) = U = 10k_BT$ which is set by the available chemical energy of $\Delta\mu \simeq 10 - 15k_BT$ for a potential period of $l \simeq 8$ nm of microtubles, this force is equal to $f_s \simeq U/l = 5$ pN consistent with the observed value at room temperature.[1] Note that the Gibb's Free Energy change for the hydrolisis of one mole of ATP is approximately 30 kj/mol corresponding to about 0.3 eV per molecule.

We will now introduce the parameters used in our model by illustrating a simple sketch of our model Fig 2.3.[3]

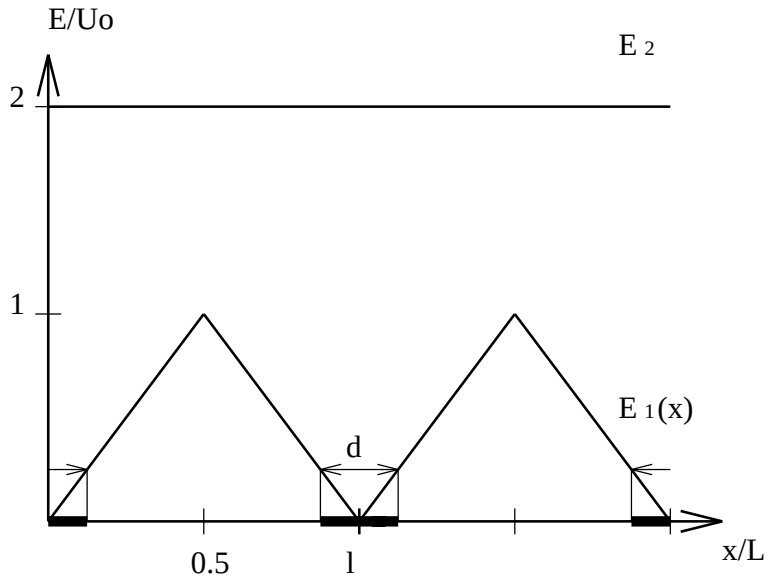

Figure 2.3: A simple diagram of E1(x) and E2 potentials. The width of the region where ATP excitation occurs is $d = 0.1$ and U_o is the height of the ratchet potential with respect to which length and energy are scaled.

If the probability densities $P_1(x,t)$ and $P_2(x,t)$, for transition frequencies w_1 and w_2 and velocity v, one can write the equation of motion for the two state

model as,

$$\partial_t P_1 + v\partial_x P_1 = -\omega_1 P_1 + \omega_2 P_2 \quad (2.14)$$

$$\partial_t P_2 + v\partial_x P_2 = \omega_1 P_1 + \omega_2 P_2 \quad (2.15)$$

$$(2.16)$$

with the use of conservation of total probability, $P_1 + P_2 = 1/L$,

$$\partial_t P_1 + v\partial_x P_1 = -(\omega_1 + \omega_2)P_1 + \omega_2/L \quad (2.17)$$

can be deducted. The equation of motion for N particles in the presence of friction may be written as,

$$NMd^2x/dt^2 = -N\lambda dx/dt - \Sigma_i dU(x_i)/dx_i + NF_{ext}, \quad (2.18)$$

where λ is the coefficient of friction. The external force F_{ext} (per unit motor system length) is the force with which the motor system does work on an external agent. σ_i is 1 if particle is in the first energy state and 0 if it is in the second. U is the ratchet potential. Note that the time derivatives of all of the x_i's are the same since the motor particles are assumed to be connected rigidly to one another. So, external force F_{ext} necessary to keep the system moving with a constant velocity is

$$F_{ext} = < \Sigma dU(x_i)/d(x_i) > +\lambda v. \quad (2.19)$$

The average value $< \Sigma dU(x_i)/d(x_i) >$ may be evaluated as an integral weighed with $P(x)$ as in the above equation because of the assumption of uniform distribution of the motor particle over the ratchet potential. For the steady state solution, $\partial_t P_1 = 0$ so that

$$v\partial_x P_1 = -(\omega_1 + \omega_2)P_1 + \omega_2/L \tag{2.20}$$

with solutions of the form $P_1 = \Sigma P_1^n$ satisfies the recursion relation $P_{1n} = \partial_x P_1^{(n-1)}/(\omega_1 + \omega_2)$ with $P_1^0 = \omega_2/(\omega_1 + \omega_2)L$. This solution of P_1 with Taylor like expansion results in,

$$f(v) = F_\Omega^{(0)} + (\lambda + F_\Omega^{(1)})v + \Sigma... \tag{2.21}$$

where $F_\Omega^{(n)} = \int P_1^{(n)} dE1(x)$ where $f(v)$ is the external force. For a symmetric potential as in our case, even terms drop, and thus we get

$$F_{ext} = (\lambda + F_\Omega^{(1)})v + F_\Omega^{(3)}v^3 + O(v^5), \tag{2.22}$$

which gives the behavior shown in Fig 2.4. One can identify a critical value for Ω above which the motor develops spontaneous motion.

For spontaneous oscillations, one should remind the reader that this phenomenon is observed in some insects as was mentioned in introduction. So, with the inclusion of a spring constant term $-kx$ in the equation of motion (for elastic coupling to the environment), one obtains

$$v = 1/\lambda \left(-\int dx - P_1 U'(x) + F_{ext} - kx \right), \tag{2.23}$$

and in the adiabatic limit behavior of the external force,

$$dv/dt = -kv/\lambda \tag{2.24}$$

can be assumed. And for a small spring constant k, the $-kx$ term can be ignored and oscillatory instability occurs for $\lambda + F_\Omega^{(1)} < 0$ as can be checked from the equation (2.20). This is valid for the area under the curve in Fig 2.5 below.[1]

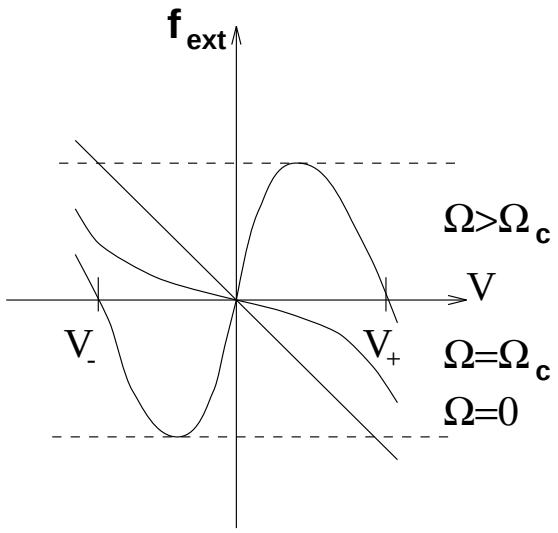

Figure 2.4: Relationship between velocity v and the applied force F_{ext}, see F.Jülicher, Ref[1].

For solutions of the sort $P_1 = P_1^0 + p(x)\exp(st)$ where $s = i\omega + \tau$ and with $v = u \exp st$ one gets

$$P(x) = -udP_1^0/dx/(\omega_1 + \omega_2 + s), \tag{2.25}$$

and for the adiabatic approximation,

$$\lambda + k/s = -\int dx(P_1^{0\prime}U(x)'/(\omega_1 + \omega_2 + s)). \tag{2.26}$$

So, the sign of τ determines the status of instability. For $\tau < 0$, the state is locally stable and it becomes unstable for $\tau = 0$. The condition on λ and k

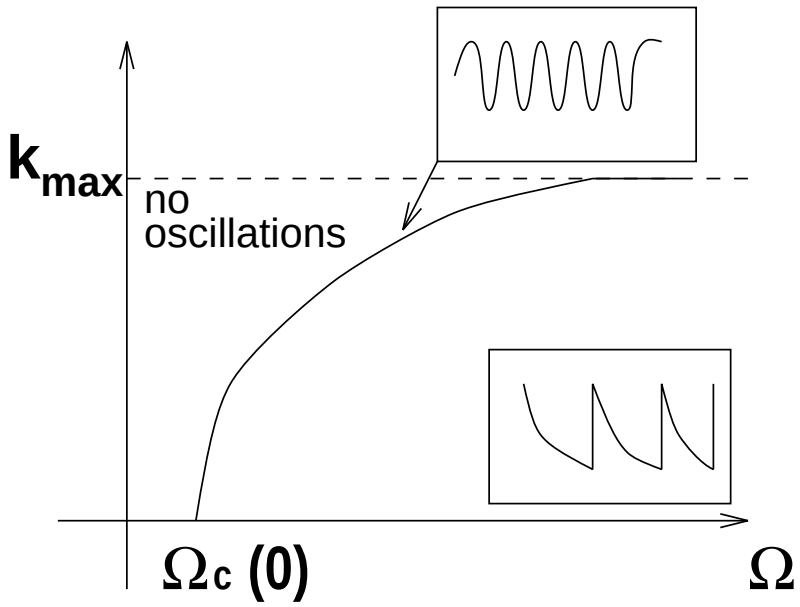

Figure 2.5: Phase diagram for spontaneous oscillations as a function of the excitation amplitude and the modulus per motor k, see F.Jülicher, Ref[1].

can be determined via integral equations. Figure 2.6[4] below gives a flavor of the dynamics corresponding to different values of the parameters.

The elastic coupling of the motors to the backbone mentioned above, has been studied separately, which is also related to the generation of internal forces. On the other hand, the attachment of the motors to a rigid backbone via springs can be used to study the effects of the elasticity of the motor material itself. Strain dependence is taken into account in this manner (see A.Vilfan, E.Frey, F.Schwabl[5,6]). If x_m denotes the displacement of the motor material from the origin, x denotes the amount of strain, x_h denotes the coordinate of

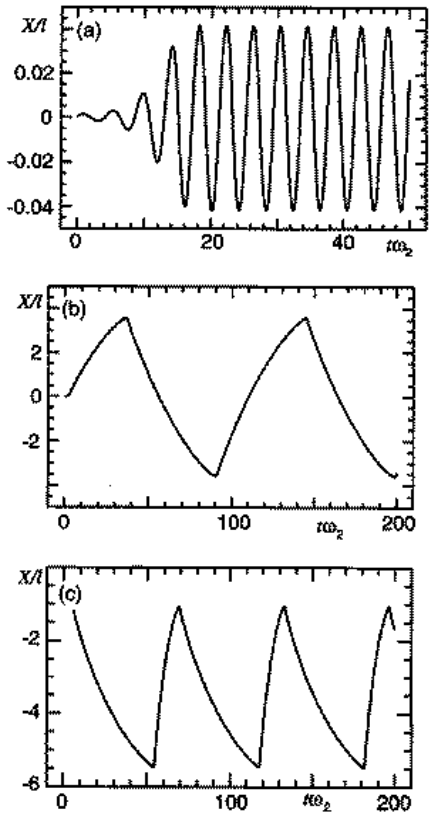

Figure 2.6: X versus t for (a) a/L=0.5, d/L=0.1, $\Omega = 0.1$, $\lambda\omega_2 L^2/U = 0.1$, and $kL^2/U = 0.2$ (b) same system but $kL^2/U = 0.002$,(c) asymmetric system a/L=0.1 for $kL^2/U = 0.01$, see F.Jülicher and J.Prost, Ref[4].

the motor particle and d_m is a measure of equilibrium coupling to backbone, the consideration is depicted in Figure 2.7.

One can assign characteristic life-times t_d and t_a for the attachment and detachment rates. Assuming Boltzmann distribution for the probability, Force and velocity ratio together with the criteria for anomalous hysteresis is depicted in Figure 2.8.

The motion of the motor when it is made of finite length particles in presence of noise has also been studied.[7] The motion of a single such particle is described

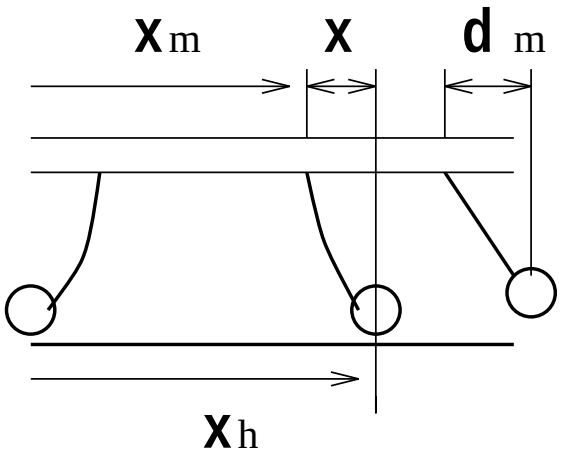

Figure 2.7: Schematic model for the motor heads running along a molecular track, see A. Vilfan, E. Frey and F. Schwabl, Ref[5].

by the Langevin equation,

$$dx_j/dt = -\partial x U(x) + \epsilon_j(t) + Asin(\omega_j t), j = 1, ..., N \tag{2.27}$$

where ϵ_j is Gaussian white noise with the auto-correlation function which satisfies $< \epsilon_j(t)\epsilon_i(t') >= 2kT\delta_{ji}\delta(t-t')$. Since in most of the experimental situations we

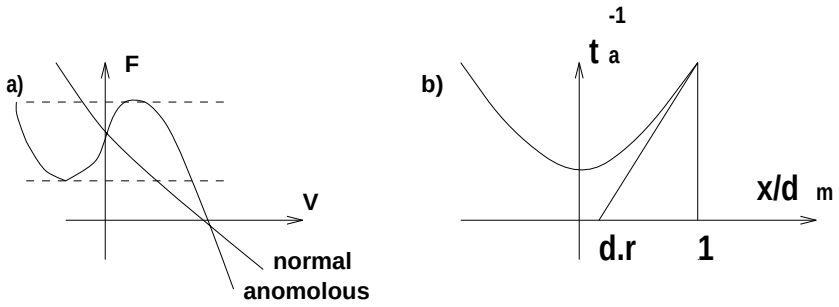

Figure 2.8: (a) F-v relation,(b) Anomalous hysteresis criteria when intersection of the tangential with the x-axis is to the right of the duty ratio. (Deformation is described in terms of harmonic potential, detachment rate t_a^{-1} is constant which is in fact strain-dependent for myosin, see A. Vilfan, E. Frey and F. Schwabl, Ref[5].

can suppose that the interaction between two particles can be well approximated with a hard core repulsion, one can assume that the particles are hard rods (Figure 2.9). They study ω and b dependence of velocity. It should be noted that our finite size analysis differs than the considerations in the above study.

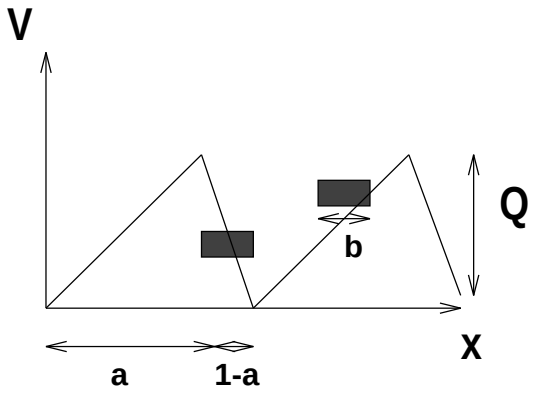

Figure 2.9: Two particles with size b subject to the saw-tooth shaped periodic potential is $p = 1$, the lengths of the slopes are $\lambda = a$ and $\lambda_2 = 1 - a$. The height of the potential is Q, see Imre Derényi and Tamas Viscek, Ref[7].

Chapter 3

DEFORMATION IN COOPERATIVE MOLECULAR MOTORS

In this and the following chapter we present the main results of this thesis. This chapter involves the analysis of elasticity in the system, while the next one will be related to finite size effect.

We have investigated the deformation on cooperative molecular motors. We analyzed motor motion in the presence of an elastic coupling between the motor particles. This contribution is implemented through an Ising-like modeling in which the elastic energy is assumed to have discrete values based on the attachment state of neighboring motor particles, ignoring the lateral stretch. The texture of the dynamics is garnished via this procedure and inter-dependencies between various dynamical variables are investigated.

Our model is based on a triangular symmetric saw-tooth potential for the track filament of the motor and a higher constant potential for the backbone as was first introduced by Jülicher[1] (Figure 2.3). We extend this model to include

elastic interactions between the modules of a system, as shown in Figure 3.1. Here, $E_1(x)$ and E_2 are the ratchet potential and constant potential respectively. The energy of the system is given by:

$$H = \sum_i (1 - S_i)E_1(x_i)/2 + \sum_i (1 + S_i)E_2/2 - \epsilon/4 \sum_{<ij>} S_i.S_j \qquad (3.1)$$

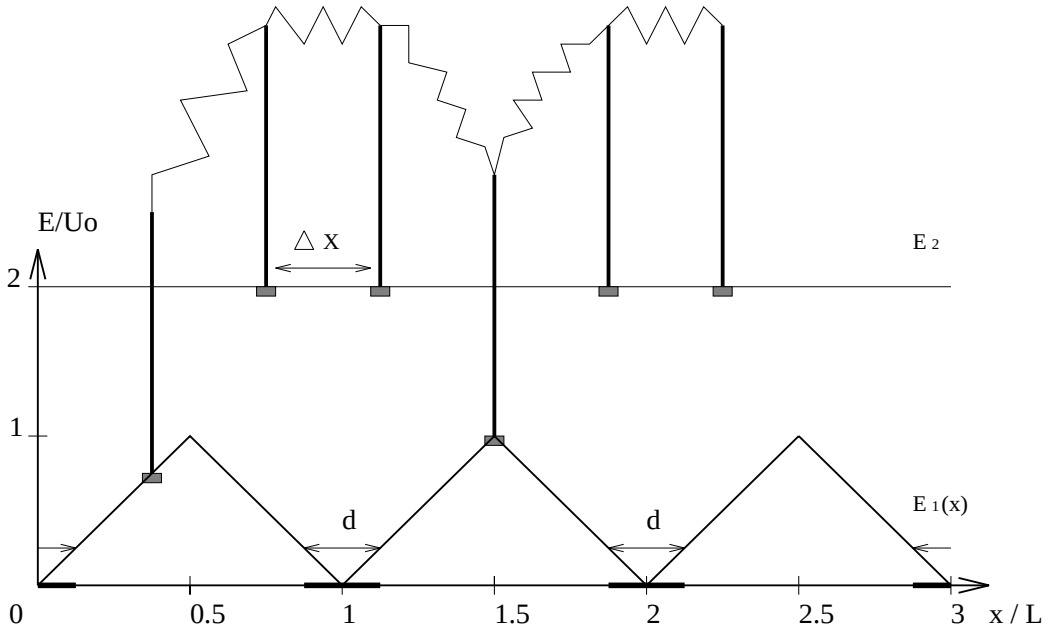

Figure 3.1: A diagram of the $E_1(x)$ and E_2 potentials. The width of the region where ATP excitation occurs is d=0.1 and U_o is the height of the ratchet potential, see Taneri and Yalabık, Ref[2].

where ϵ is a positive constant, which denotes the amplitude of the potential representing the deformation energy. S_i indicates the state of the i th particle with $S_i = -1$ for the detached and $S_i = +1$ for the attached states and the sum over $< ij >$ indicates a summation of over all nearest neighbor pairs. One should note that the deformation energy is increased by an amount $\epsilon/2$ when the adjacent particles are in different states of springs stretched in comparison to the case when they are in the same state (springs not stretched).

In our generalization of the model, the major effect of the deformation is

assumed to be related to the states of the particles i.e. attached or detached. Admittedly, a deformation might correspond to a displacement of the particles relative one another in the direction of the motor motion. In this work, we are considering a limit in which such relative displacement results in small changes in energy and hence in transition rates in comparison to changes resulting from being in attached or detached states.

Both attractive and repulsive forces can occur between various protein membranes. Repulsive forces arise between proteins if they have a strong affinity for the lipids, for example, via ionic bonds. Attractive forces arise if the proteins can bind to each other, e.g., via Ca^{2+} or molecular bridges and via Van der Waals forces.[8] In our case of deformation, attractive forces between the protein particles within the filament are being modeled via springs and forces between the filaments should be considered as ionic.

We carry out a Monte Carlo simulation of this system using the dynamics given by the transition rates.[4,9,10]

$$\omega_1(i) = w_2 \exp[(\epsilon(S_{i+1} + S_{i-1})/2 + E_1(x_i) - E_2)/kT] + \Omega(x_i) \qquad (3.2)$$

where $\omega_1(i)$ is the transition rate for the i th particle from the attached state to the detached state. The transition rate for the reverse process ω_2 is chosen as 0.5 and defines the time scale. Note that $\Omega(x_i)$ destroys the detailed balance and represents the ATP excitations.[9] This effect is assumed to be present at certain regions on the track, as shown in Figure 3.1. We call Ω as the "excitation amplitude" for consistency with the previous work.[9] We take $\Omega = 5$ a value sufficiently large compared to the time scale defined by ω_2. Note that, k and T are the Boltzmann constant and the temperature respectively. The function of the motor relies on the release of energy from the particles to one side of the potential ramp, while they are being detached from the other side by excitation. Motion of a motor makes it more probable to release its energy on the side of the potential ramp, which enhances the motion in that direction. This leads to

a dynamical instability and hence a spontaneous velocity.

The correlations generated by the deformation energetics result in more of the excited motors reaching the "other side of the ramp", which yields a better collective, motor performance for some range of parameters. On the other hand, these correlations make an analytical analysis of this system prohibitively complicated.

The numerical computation was started by assigning the motor an initial velocity. The motor is assumed to consist of 1000 particles separated by an amount Δx on a ratchet potential with period L. The force acting on the protein was then calculated at each time step. The total collective motor force (F_{mot}) due to potentials indicated in Figure 3.1 is determined by adding up the forces for both attached and detached particles. (The force on a detached particle is trivially zero whereas the force on an attached particle is negative the slope of the model symmetric saw-tooth potential.) The motor is moved at the initial constant velocity v, and the force acting on the individual motors is averaged over. The inter-particle distance Δx is irrational multiple of L so that the distribution of the motors is incommensurate with L. This guarantees that for a sufficiently long filament the motors will be distributed uniformly over the potential period and therefore the force will be constant. The state of the motors was changed at each time step by the following procedure:

The total probability of any transition in a time interval Δt is calculated,

$$P = \Delta t \sum_i \omega_j(i), \tag{3.3}$$

where $\omega_j(i)$ is the transition rate of the i th motor in j th state in the system. The time step Δt is chosen such that the total probability P is much less than unity so that the probability of more than one transition in Δt is negligibly small.

Whether or not a transition will take place is decided at each time step with probability P. The particular state, which will go through the transition is chosen

randomly with a probability proportional to its transition rate.

The motor force F_{mot} is calculated at each time step, and the sequence of states obtained as described above are used to form an average of this quantity. (In order to comply with this constraint F_{mot} is calculated through 10^5 time steps of $\Delta t = 10^{-3}$ the system is sufficiently relaxed, except for large values of ϵ where averaging is done through 10^6 time steps of $\Delta t = 10^{-4}$).

In order to use dimensionless quantities, we scale the lengths by the period of the ratchet potential L, the energies by the magnitude of the variable is then scaled by $\sqrt{ML^2/U_0}$. We have chosen the energy of of the detached and attached states as $E_2/U_o = 2$, and $kT/U_o = 1$. The inter-particle distance Δx is chosen as $\sqrt{2}/4$. As an example for the actual value to this parameter, one considers kinesin, for which $\Delta x/L$ is typically around 0.24, given the motor density is $5 \times 10^8 m^{-1}$, (see reference [11]) and potential period is 8.2nm.[12]

The force developed by the motors as a function of v for different values of ϵ will be of the form shown in Figure 2.4 with $\Omega > \Omega_c$ (where Ω_c is the critical excitation amplitude) with the exception that friction force $F_f = -\lambda v$ is to be subtracted, $F_{mot} = F_{ext} + \lambda v$. For intermittent values of ϵ, the introduction of correlations results in enhancement of attached and detached particle domains in accordance with the states the adjacent particles are in. For small values of Δx, these adjacent motors are more likely to be on the same ramp. For very large values of ϵ however, ATP excited adjacent motors tend to stick to their excited states so that the mechanism generating the force is now blocked. It should be remembered that the friction coefficient λ cannot be larger than a critical value λ_c for any particular value of ϵ, if the system is to function as a motor.

According to Figures 3.2 and 3.3, we see that "maximum collective motor force" F_{max}, and λ_c increase with increasing ϵ. But, for large values of ϵ we see a drop in both F_{max} and λ_c since the large increase in correlation spurs attached particles to the upper constant energy level, which inhibits force generation. The

decrease in velocity at F_{max} as correlation increases is not surprising since the increase in ϵ enables the particles to remain in their excited states for a longer time. This energy can be supplied to the motor especially if it travels with a lower velocity.

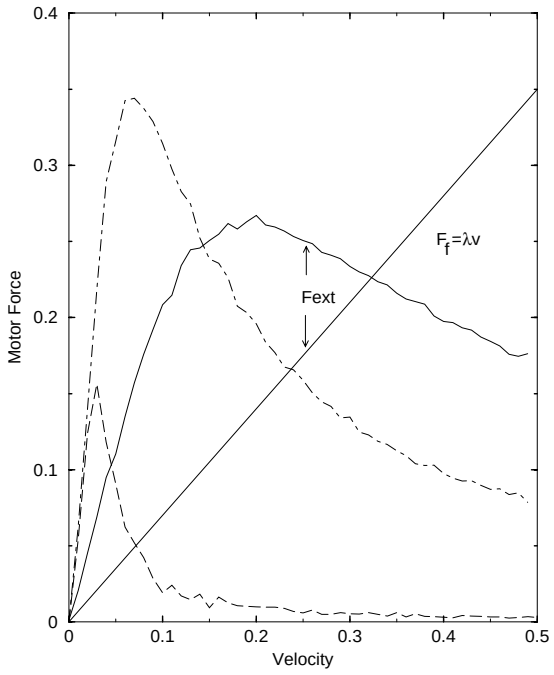

Figure 3.2: The velocity dependence of the F_{mot} for ϵ=0 (solid), ϵ=4 (dot-dashed), ϵ=8 (long-dashed) for inter-particle distance $\Delta x = 0.09$

The inter-particle distance dependence of F_{max}, for different ϵ values is displayed in Figure 3.4. For non-zero ϵ and small values of Δx, the inter-particle distance, F_{max} increases, while for the values of Δx around half the spatial period, F_{max} decreases. This is in contrast to the $\epsilon = 0$ case where F_{max} stays constant as expected because, the particle distribution is uniform and incommensurate in the absence of correlations. The size of the fluctuation gives an idea about the magnitude of systematic errors due to finite length of our system.

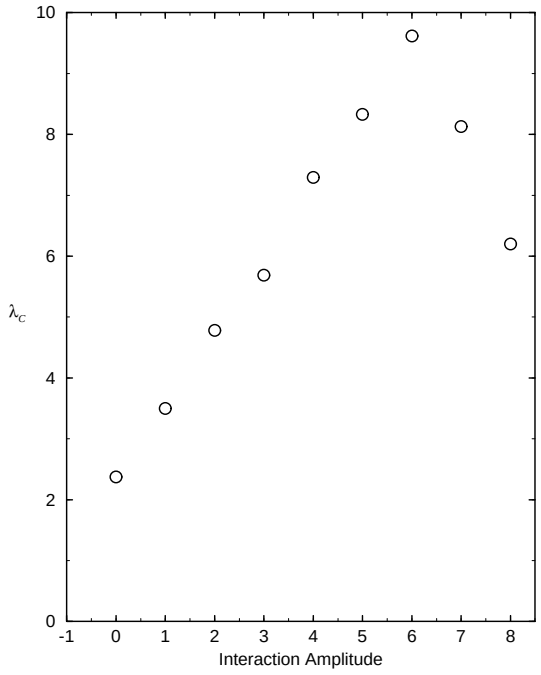

Figure 3.3: The critical value of λ, λ_c versus the interaction ampli tute ϵ for $\Delta x = 0.09$.

The population of particles in the attached states is shown in Figure 3.5. It is seen that the population pattern is deformed for larger inter-particle distances. To understand the multiple peaked structure of the $\Delta x = \sqrt{2}/4$ graph, consider the problem of arranging three adjacent particles to obtain a maximum amount of force. For this inter-particle distance one cannot have all three adjacent particles attached to the symmetric saw-tooth potential so that all three experience a positive force. This explains why F_{max} decreases for values of Δx around half the spatial period in Figure 3.4, since one can have all three adjacent particles experience a positive force due to the saw-tooth potential. Now, for inter-particle distance $\Delta x = \sqrt{2}/4$, there are three intervals for the central particle in which two of the three particles experience a positive force while avoiding the ATP present regions. We expect to see a population growth in these intervals so that the motor attains F_{max}. Indeed, Figure 3.6 shows how this results in three peaks, which are responsible for the deformation shown in Figure 3.5. One can also

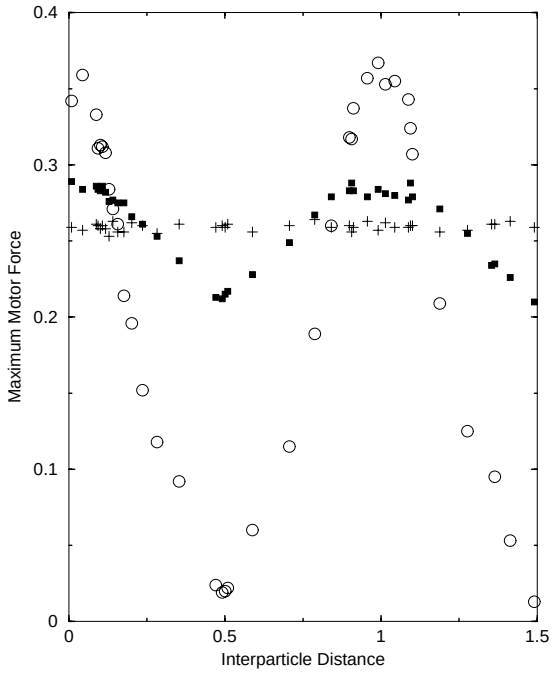

Figure 3.4: The inter-particle distance dependence of F_{max} for $\epsilon = 4$ (circle), $\epsilon = 1$ (small-filled circle) and $\epsilon = 0$ (plus). We have extended the plot beyond the expected period of $\Delta x = 1$, as a check of our computation.

see that the overwhelming contribution to the total force comes from triplets of neighboring motors all in attached states.

The ϵ dependence of F_{max} is studied in Figure 3.7, which simply summarizes the dynamics of the system examined earlier. The error bars in Figure 3.7 have been determined through a somewhat optimistic estimate, dividing the mean square fluctuations of the measured quantity by the square root of the number of independent samples in the average. This number has in turn been estimated as the total simulation time divided by $3/\Omega$, which is one of the time scales in the system. In particular, systematic errors which may be the result of the finite size of the system are expected to be small and not included in this analysis.

We have also looked at the efficiency of the process, as defined by the duty

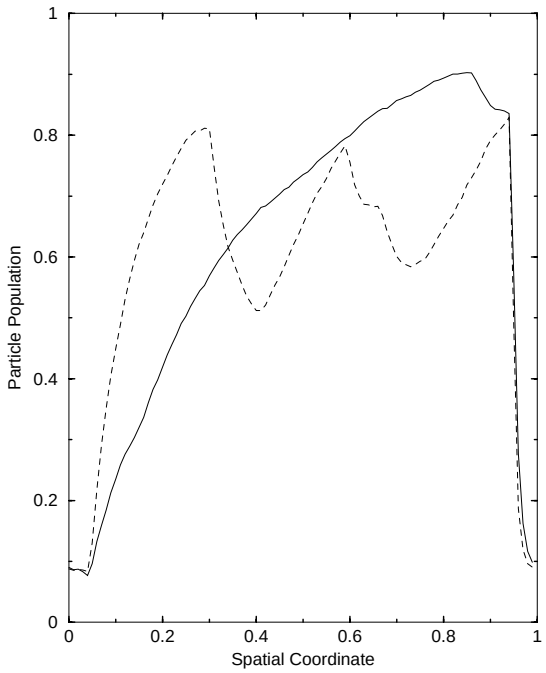

Figure 3.5: Population versus spatial coordinate of the particles attached to the ratchet potential at maximum motor force and for inter-particle distances $\Delta x = 0.09$ (solid) and 0.36 (dashed) with $\epsilon = 4$.

ratio of the power delivered by the collective motor to the total power supplied by the ATP excitations.[1] Consistent with our results we find that the efficiency of the finite ϵ collective motor is larger than that for $\epsilon = 0$ at smaller values of the velocity.

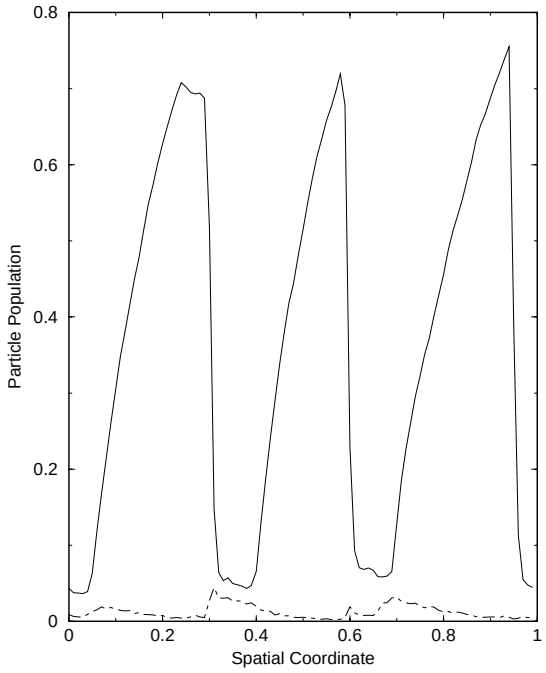

Figure 3.6: Population versus spatial coordinate of a triplet of neighboring particles all attached to the ratchet potential (solid), and with central particle attached while both of the neighbors detached (dot-dashed) at maximum motor force. Inter-particle distance $\Delta x = 0.36$ and $\epsilon = 4$.

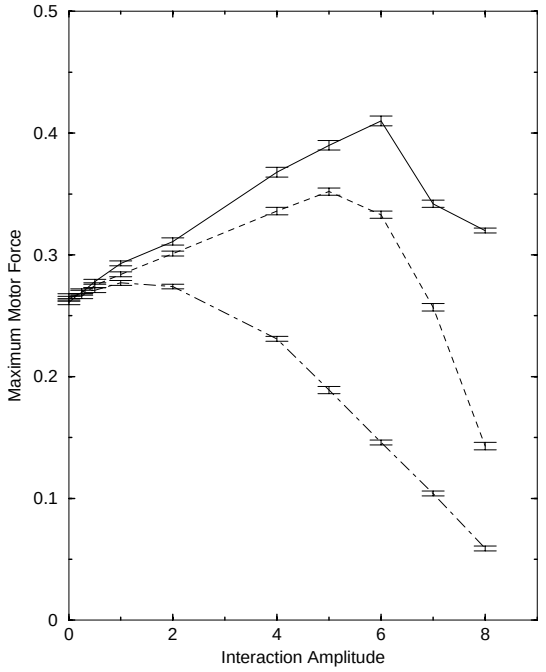

Figure 3.7: F_{max} versus interaction amplitude ϵ for three different inter-particle distances $\Delta x = 0.04$ (solid), 0.09 (dashed) and 0.18 (dot-dashed).

Chapter 4

FINITE SIZE EFFECTS IN COOPERATIVE MOLECULAR MOTORS

In most theoretical studies of motor proteins, the size of the system is assumed to be very large, or infinite so that they may be considered as rigid backbones sliding with a constant velocity on ratchet like potentials.[1,12,13] Such large size, in the presence of an incommensurate ratchet potential implies a uniform distribution of the particles over the period of the potential, and simplifies the analysis considerably.

The uniform distribution also eliminates the fluctuations in the effective incommensurate force experienced by the chain, resulting in uniform motion. We have aimed to study the effects introduced by finite size, which turned out to be significant for these systems. Other studies of Imre Derényi and Tamas Viscek for finite length particles were mentioned in section II.

We begin our study by looking at a molecular motor system, which is made up of a finite number of particles. The force experienced by the motor filament as

it moves on the ratchet potential is no longer uniform. This would then indicate a non-uniform motion of chain, and we have studied the characteristics of this motion for the damped as well as the under damped case where the mass of the system would also be expected to play a role. Very long as well as very massive proteins would be expected to yield results close to the studies on infinite length proteins, which act as a check on our results. We have recovered the previously reported results for the infinite chain length limit.

The two-state model we have used includes a symmetric ratchet potential for the track on which the particles are attached, and a constant potential (see Figure 2.3). As discussed earlier the detailed balance is broken through one-way ATP excitations. Therefore, one can see a spontaneous motion even when the ratchet potential is symmetric. We display the fluctuations in the sliding velocity. In this work, we study motors made up of a small number of particles, in which case a continious distribution of particles can no longer be assumed. In fact for such small systems, the sliding filament is expected to feel a set of discrete values of forces. We simulate these finite systems through the Langevin equation. While the infinite (in mass or size) system implies a perfect statistical averaging, fluctuations appear in finite systems.

The motion of the motor is governed by the Langevin equation with mass included;

$$NMd^2x/dt^2 = -N\gamma dx/dt - \sum_i dU(x_i)/dx_i - \sum_i \epsilon_i(t) \qquad (4.1)$$

with the assumption that all particles have the same mass and that the inter-particle distance does not change so that the velocity dx/dt is same for all of the particles. Here, N is the number of particles, x_i is the position of the i th particle, $U(x_i)$ is either $E_1(x_i)$ or E_2 depending on which potential level the particle is in. Due to viscous damping, which may be due to external or internal forces, there is a friction force with damping coefficient γ per particle. $\epsilon_i(t)$ is Gaussian white noise with correlation function $< \epsilon_i(t)\epsilon_j(t') >= 2D\delta_{ij}\delta(t-t')$ with zero mean $2D$ is the noise strength with $D = \gamma kT/NM^2$, see reference [13]. We limit our study

to number of particles $N =\leq 10$.

We again use dimensionless quantities such that lengths are scaled by the period of the ratchet potential L, energies by the magnitude of the potential U_o and masses by the mass of a protein particle M_o. The time variable τ is then scaled by $\tau_o = \sqrt{M_o L^2/U_o)}$. Then for $M = M_o$ and $u = U/U_o$ equation (3.4) can be rescaled and written as,

$$N d^2x/dt^2 = -N\Gamma dx/dt - \sum_i du(x_i)/dx_i - L/U_o \sum_i \epsilon_i(t) \tag{4.2}$$

where $\Gamma = \gamma\tau_o/M_o$. With this scaling, we have chosen the energy of the detached state as $E2/U_o = 2$ or 1.5, and $kT/U_o = 1$ for our computations. inter-particle distance Δx is taken to be incommensurate with the ratchet period as $\sqrt{2}/2$ and $\sqrt{2}/4$. We choose $M/M_o = 1.2$ and $\gamma = 0.1$. The numerical procedure starts with the same procedure as for the deformation case. The motor is moved at the constant initial velocity for a time period of $\tau = 2$. At the end of this period it is assumed that the distribution of particle states is sufficiently close to steady state. The analysis here is conducted through time steps of $\tau = 2 \times 10^{-3}$. After the initial 10^3 time steps, the total force acting on the motor at each time interval due to the ratchet potential is calculated. Use of this total force together with the friction and the white noise enables one to solve equation (3.5) numerically (finite increments method).[13] Using the procedure described at each time step, one can find the velocity of the motor as a function of time. During this process, we use a total of $7.5 \times 10^4 - 7.5 \times 10^6$ time steps, depending on the chain length of the motor for good statistical averaging.

In the infinite length case, one finds stable solutions for velocity $V = dX/d\tau$. For finite but large N, one has finite fluctuations ratchet potential is symmetric. We display the fluctuations in the sliding velocity between $\pm V$, which average to zero. For such finite systems the motor then moves either in one direction or the other for some period of time, but then reverses its direction and the process continues. The amount of time the motor moves in one direction before reversing

its velocity is then an important parameter which characterizes the transport mechanism. We therefore studied the average time τ that the motor moves in one direction as a function of several parameters. These quantities are characterized by the number and mass of the particles, the temperature and the inter-particle distance. Note that there are two kinds of random processes acting on the motor. One is the transition of motor particles between the attached and detached states and second is additive noise. One can in principle use two different temperature variables for these two types of random events, one for the motor and the other for additive noise in noise-force equation (3.5). We have studied the system for zero and finite values of temperature for the additive noise. Our studies indicate that these two different types of noise are not additive.

For the over damped system with finite number of motors, the mass term in equation (3.5) is neglected. One then has a system whose velocity is proportional to the force. In principle, such a system can switch its velocity. In practice, such a system does change its velocity at a rate faster than the under damped systems, but this rate depends on the length of the motor. Motor system of sizes $N = 20$ and $N = 100$ were studied in this limit. The system under study is prepared in an initial optimal condition where the particles are attached or detached to the ratchet potential such that the force in the assumed direction of motion is maximum. Then, the coordinates of an ensemble of 100 such systems were followed. The stability in the velocity of a system was observed to increase with the system size.

As was discussed earlier, the finite size motor has distinctly different behavior in contrast to the infinite system. Our study indicates that velocity fluctuations are significant even for system sized of $N = 10$. The fluctuations were found to diminish exponentially with system size and mass. Our choice of a symmetric ratchet potential results in fluctuations that are symmetric in velocity, which makes the analysis easier. The velocity of the eight particle system as a function of time is shown in Figure 4.1 for the noiseless case.

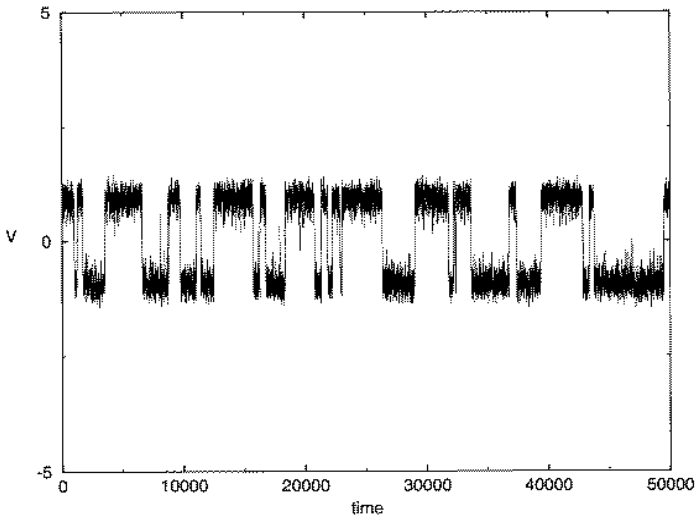

Figure 4.1: The time dependence of the velocity for N=8, $\Delta x = 0.71$ and $\Gamma = 0.09$ with $T = 0.01$.

One can easily assign an average time constant to these fluctuations. For example, the average time spent in particular direction -average switching time- is $\tau = 3125$, for the system in Fig4.1. The time scale increases exponentially with the number of particles and $1/\Gamma^2$, which is proportional to the mass of the system due to our scaling. These dependencies are shown in Figures 4.2 and 4.3, with corresponding fits $\tau \sim \exp(0.68N)$ and $\tau \sim \exp(0.26/\Gamma^2)$.

The average velocity amplitude versus system size is displayed in Figure 4.4 for two different values of inter-particle distance. We have chosen irrational values in relation to the period of the ratchet potential for inter-particle distance to generate a uniform distribution of coordinates on a period for very long chains. Apparently even the largest sized systems that we consider considered were not big enough to be completely independent of particle spacing. The inter-particle spacing dependence of average velocity is the largest for the smaller size systems as expected. The dependence of the average velocity to Γ is displayed in Figure 4.5. This gives a parabola like behavior whose V_{av} value does not change much

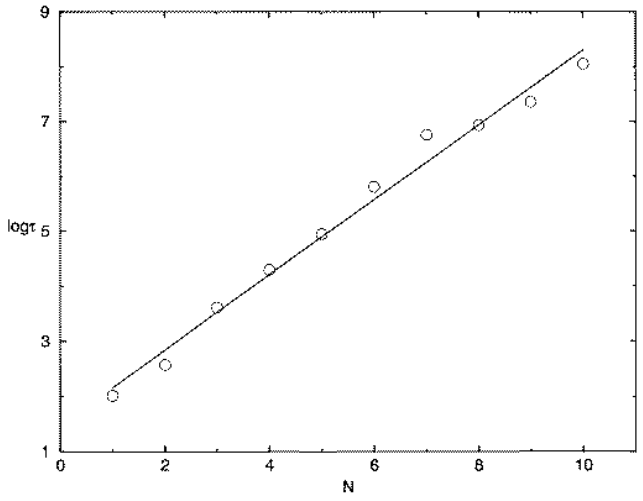

Figure 4.2: log τ versus N for Δx=0.71 and $\Gamma = 0.09$ with T=0.01 .

with variations in Δx. This is to be expected since V_{av} should decrease with increase in the damping coefficient.

We have also studied the effect of random force on the system, modeled as the thermal noise. Note that this brings a second (and in our case independent) temperature variable to the analysis in addition to the attachment/detachment process. Figures 4.6 and 4.7 display the noise temperature dependence of average switching time. Increase of noise temperature lead to an increase in the thermal excitation rate, thus giving rise to faster fluctuations in velocity. Note that the fluctuations in velocity do not disappear as this noise temperature becomes very small due to the random process associated with attachment/detachment. The rate process associated with the two different random processes do not seem to add trivially.

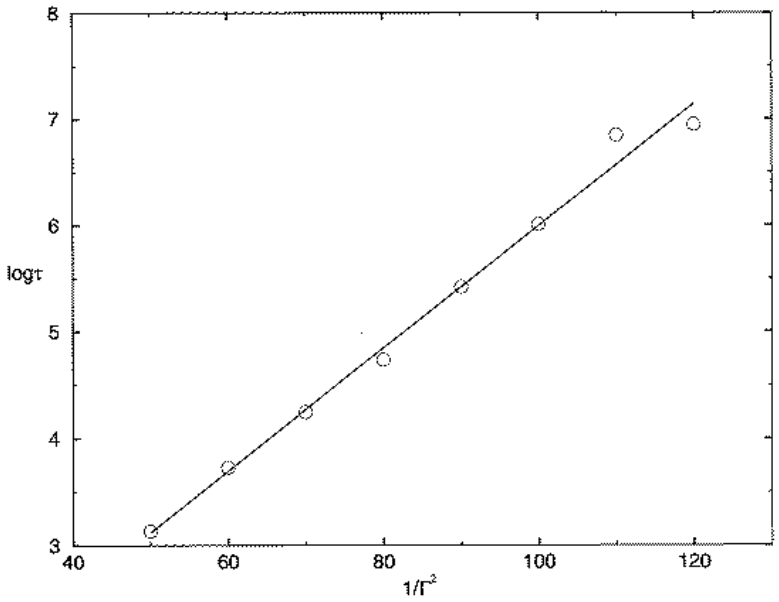

Figure 4.3: log τ versus $1/\Gamma^2$ for $\Delta x = 0.71$ and N=10 with T=0.01 .

4.1 The Asymmetric Ratchet Potential For the Over-damped Case

For the over damped ($M \cong 0$) case, an ensemble of coupled motor systems were started using the "optimal" initial condition discussed earlier. The coordinates of these systems were then followed as a function of time and are displayed in Figures 4.8 and 4.9. As can be seen from these figures, the smaller ($N = 20$) systems fluctuate in velocity in relatively short times. $N = 100$ systems also do fluctuate in velocity. A computation of the standard deviation in coordinates of the systems in the ensemble leads to the curves in Figure 4.10. It is apparent that the $N = 20$ systems eventually stop, so that the standard deviation ceases to increase, while $N = 100$ systems distribute themselves in opposite directions,

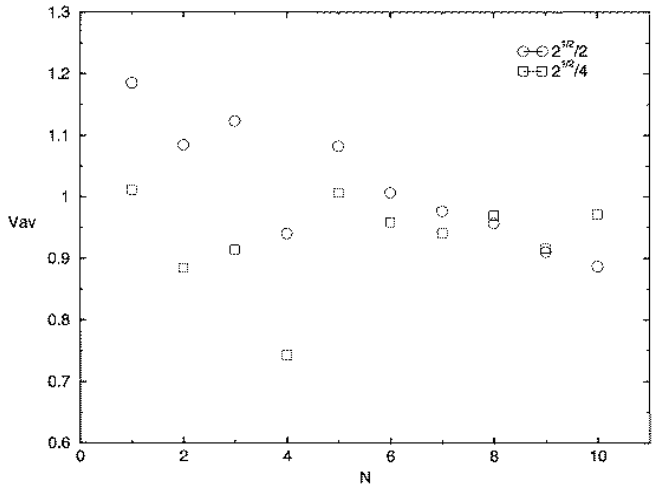

Figure 4.4: V_{av} versus N for $\Gamma = 0.09$ and $\Delta x = 0.71$.

so that the deviation increases monotonously.

It is an arising question whether the change in this behavior as a function of N is smooth or sharp.

For the asymmetric case, we take the peak of the ratchet potential at x=0.6 and the false width of the ATP region same but proportionately shared with the new slopes. One can see that the time constants for the negative velocity region gets longer for (N=8) in Figure 4.11.

For mass equals 0 asymmetric case we see a motion in negative direction in of Figures 4.12 and 4.13 since the slopes have now changed with the length of the negative slope region larger. The value of the standard deviations are now smaller for both cases since the filament has an inclination to go in the negative direction, see Figure 4.14.

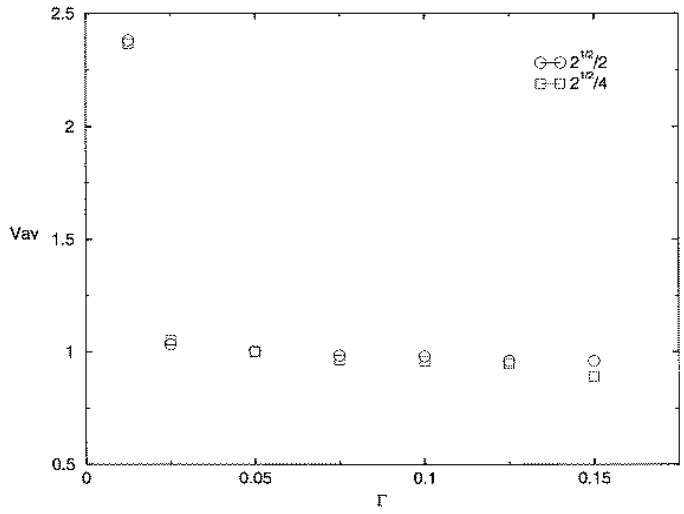

Figure 4.5: V_{av} versus Γ for $\Delta x = 0.71, 0.35$ and N=10.

For the asymmetric case we can also plot the negative direction initial condition which results in motion in negative direction and we attain decreasing x values as time proceeds as seen in Figures 4.15 and 4.16.

4.2 The Asymmetric Ratchet Potential for the Under-damped Case

We have also analyzed the under-damped model for an asymmetric ratchet potential. For different values of peak locations of ratchet potential the particle number and mass dependence of logarithm of time constant is given in Figures 4.17 and 4.18. Random patern for different Δ values, defined as the peak of the ratchet potential, is due to errors used in the method. As a matter of fact the error in time calculation is of the order of the time value itself which is found from

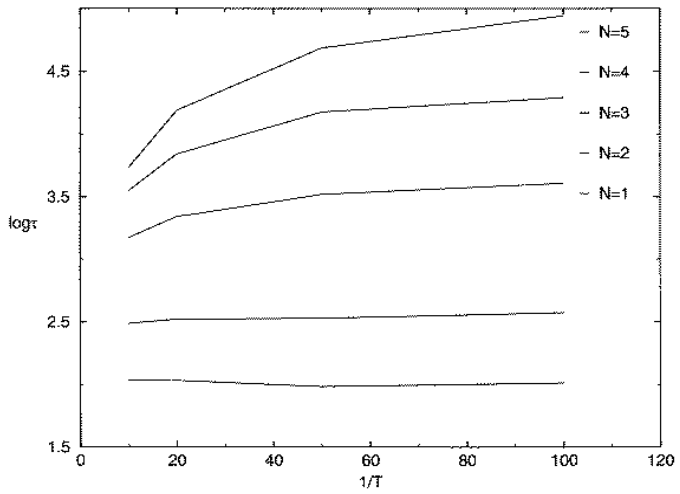

Figure 4.6: log τ versus 1/T for $\Delta x = 0.71$, N=1-5 and $\Gamma = 0.09$.

the standard deviation divided by the square root of number of time constants because of un-correlation. So, the error in log τ is of the order of 0.2.

In this case, log τ increases with N. The accuracy of our computation does not allow the analysis of any systematic dependence of τ on the asymmetric parameter Δ.

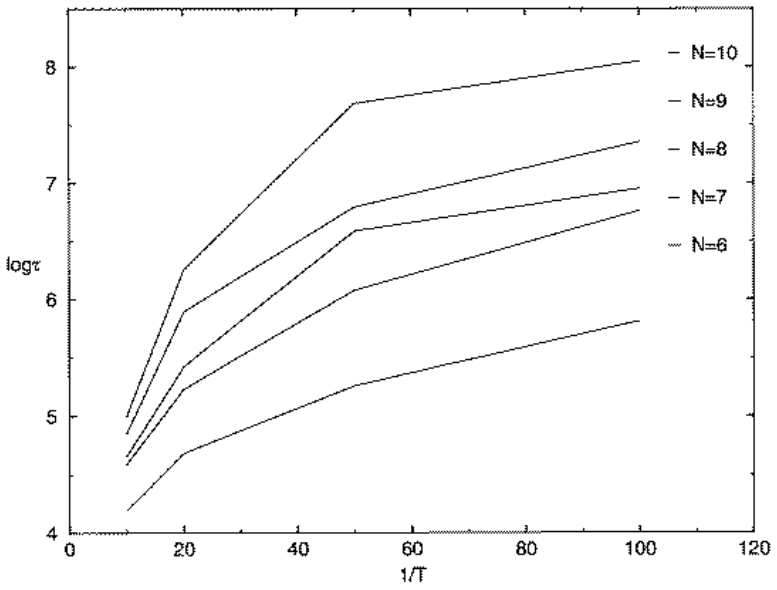

Figure 4.7: log τ versus $1/T$ for $\Delta x = 0.71$, N=6-10 and Γ=0.09.

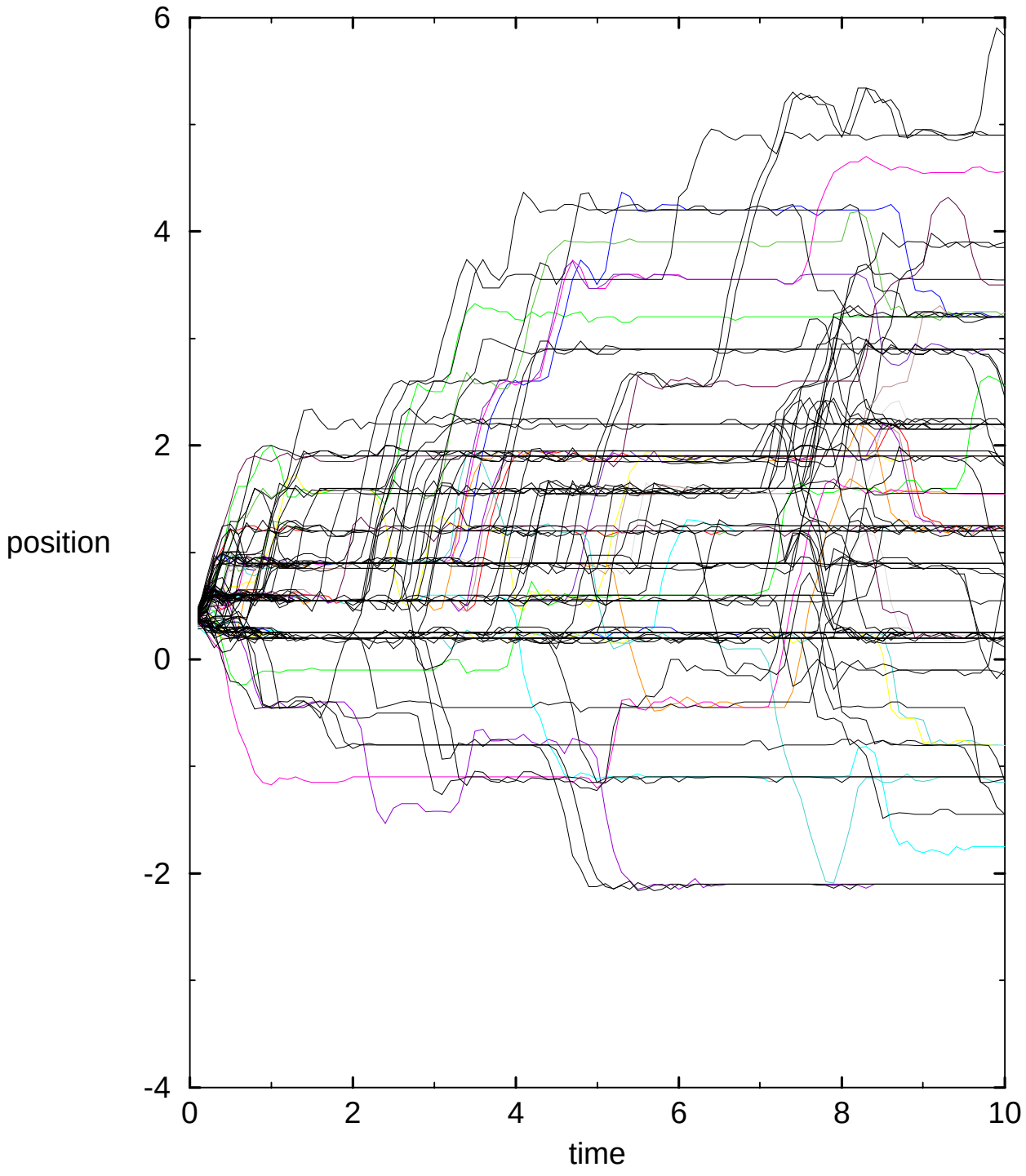

Figure 4.8: Position versus time for $N = 20$.

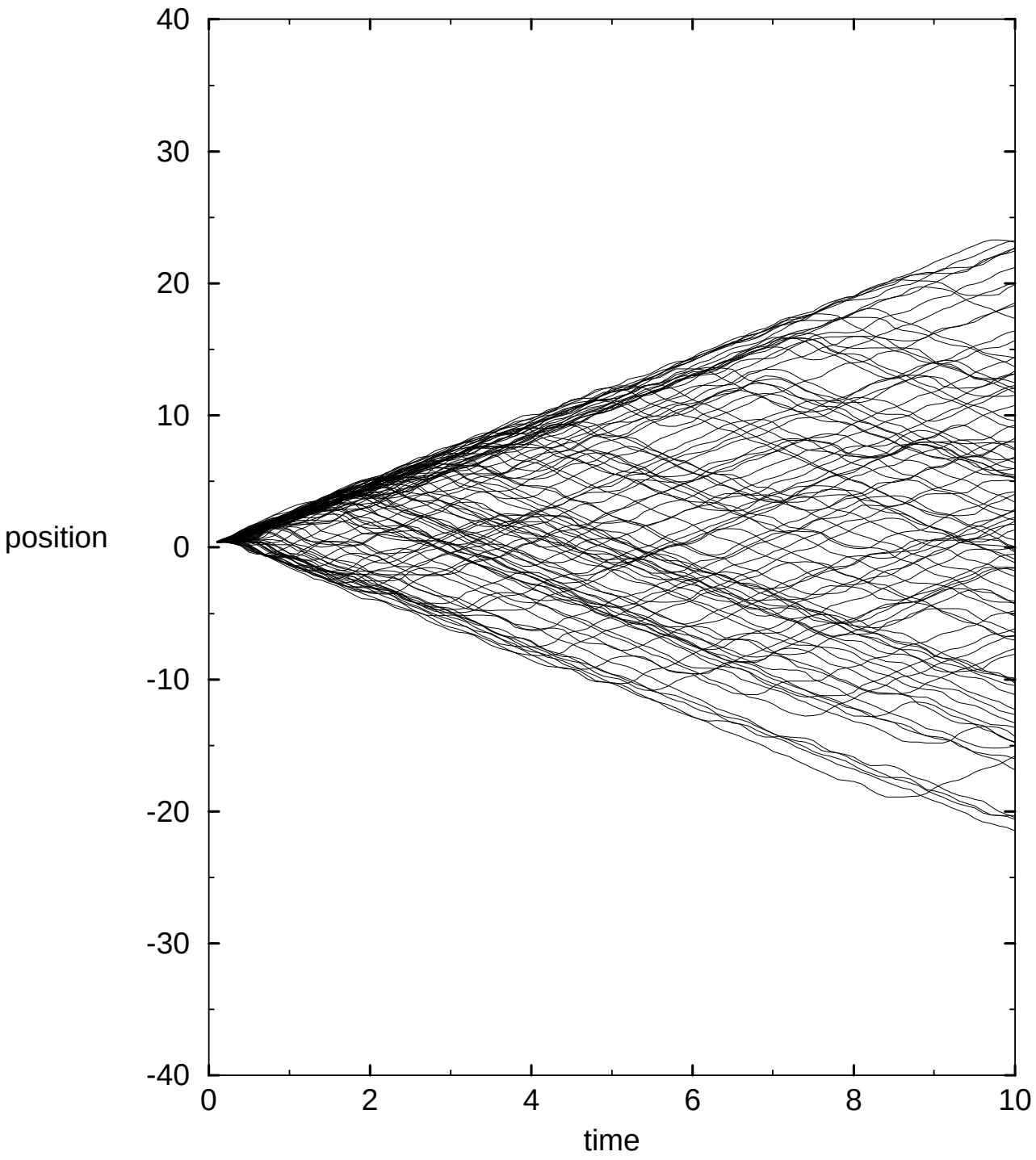

Figure 4.9: Position versus time for $N = 100$.

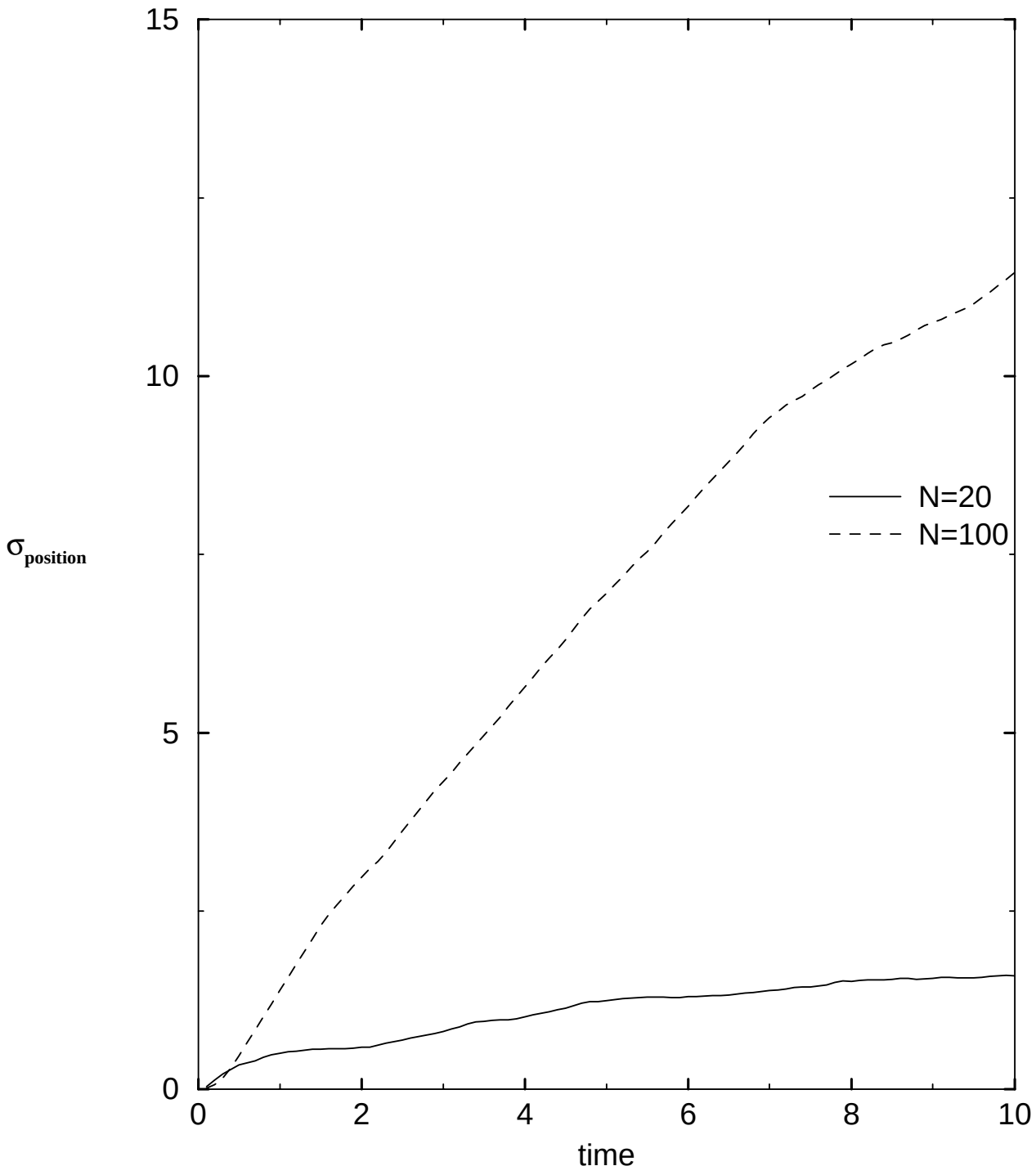

Figure 4.10: Standard deviation of position versus time for $N = 20$ and $N = 100$.

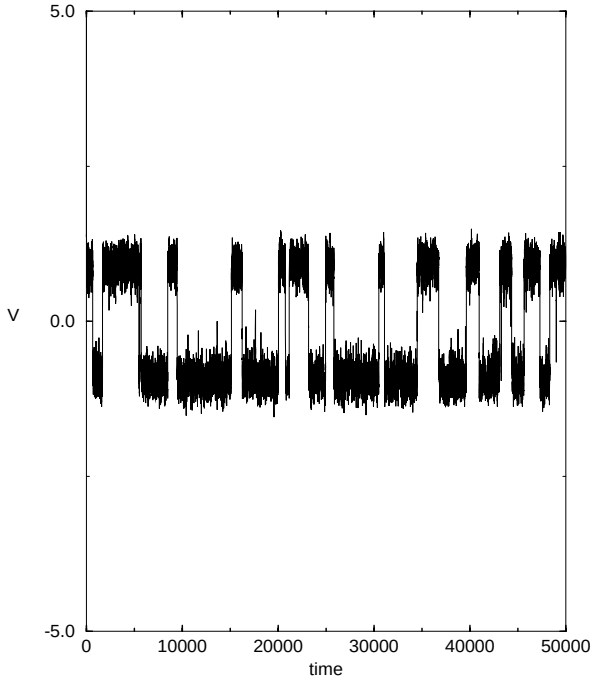

Figure 4.11: Velocity versus time for $N = 8$ and Δ=0.6.

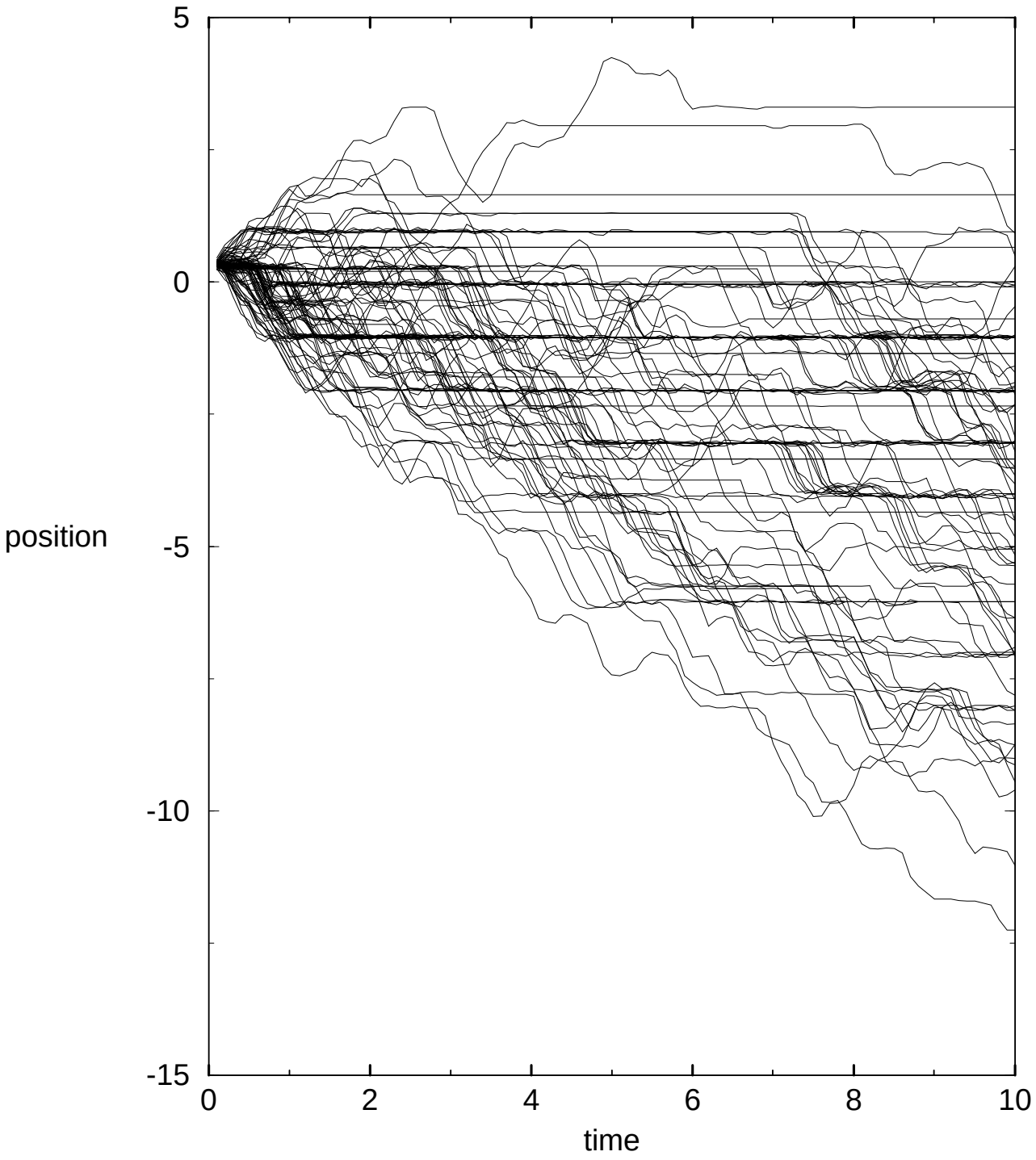

Figure 4.12: Position versus time for $N = 20$ and Δ=0.6.

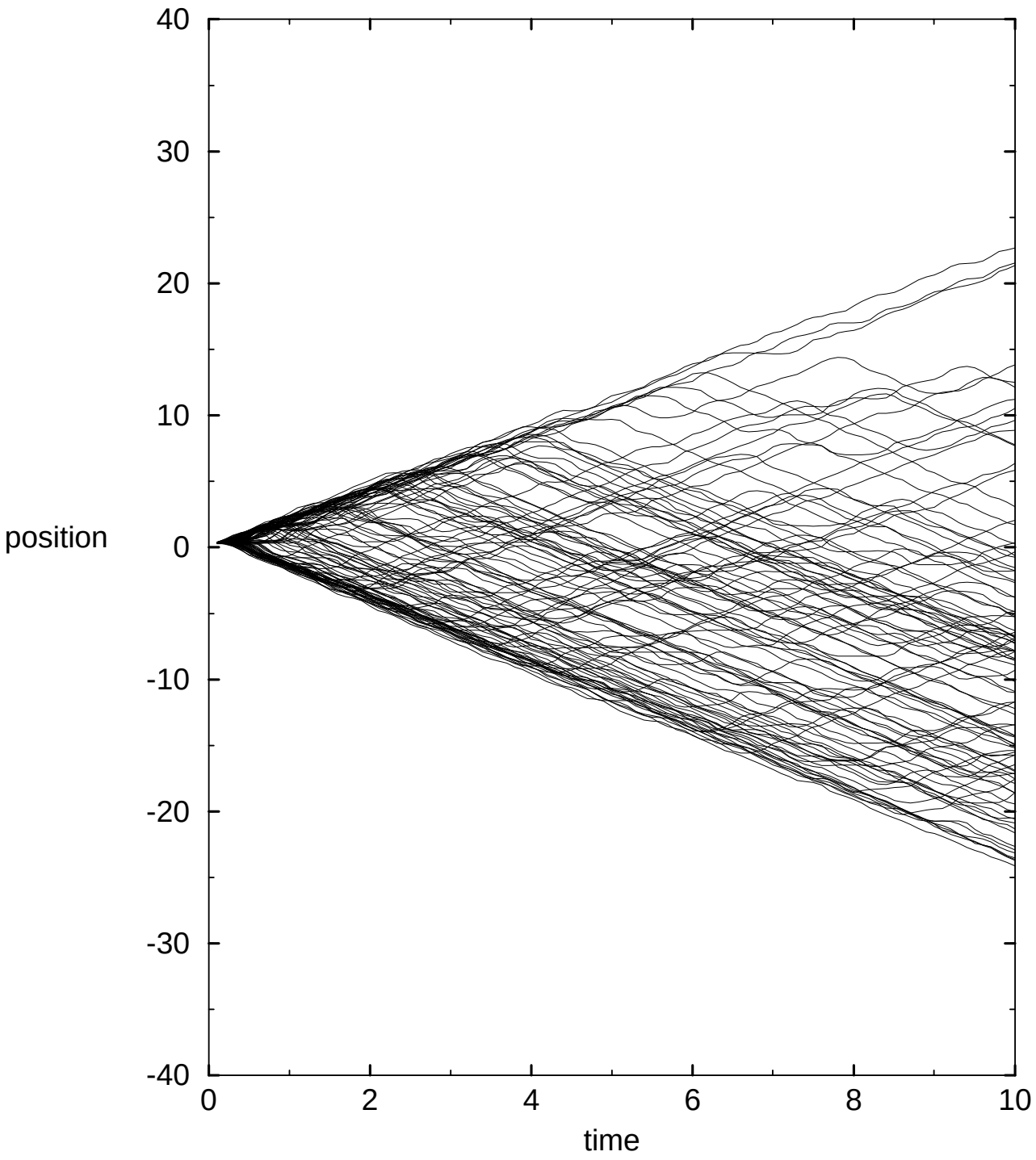

Figure 4.13: Position versus time for $N = 100$ and Δ=0.6.

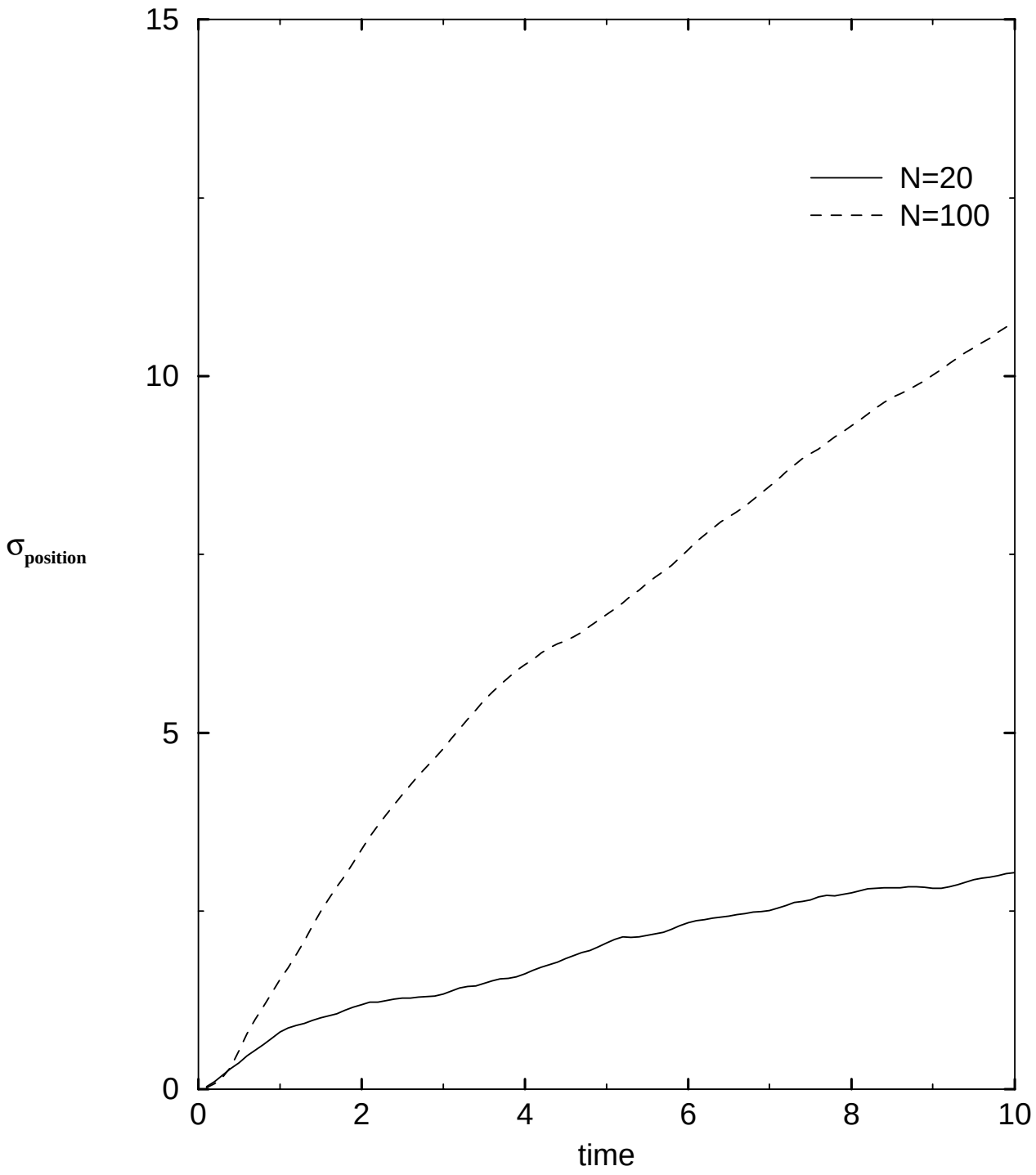

Figure 4.14: Standard deviation versus time for Δ=0.6.

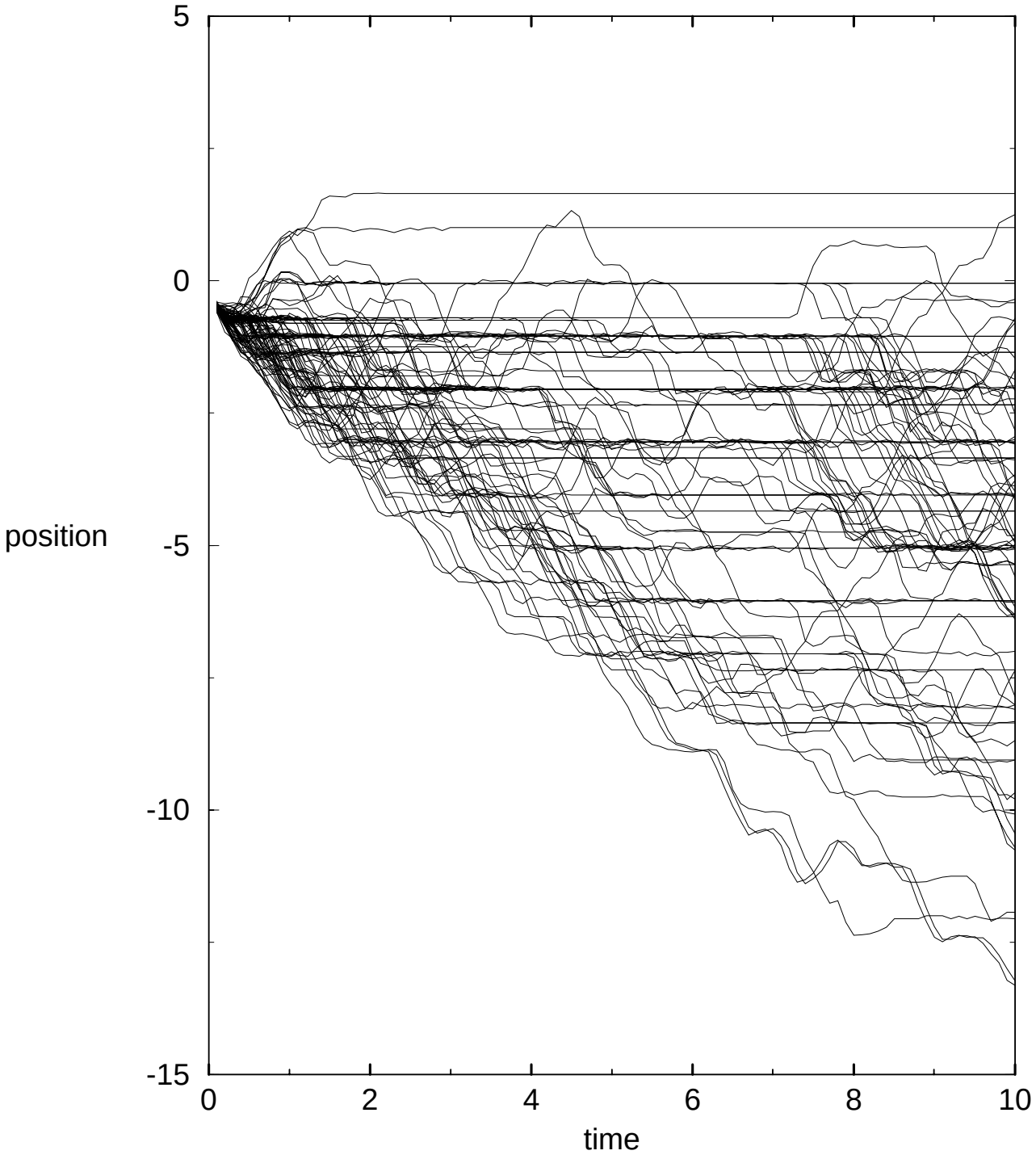

Figure 4.15: Position versus time for $N = 20$ with negative initial direction and $\Delta = 0.6$.

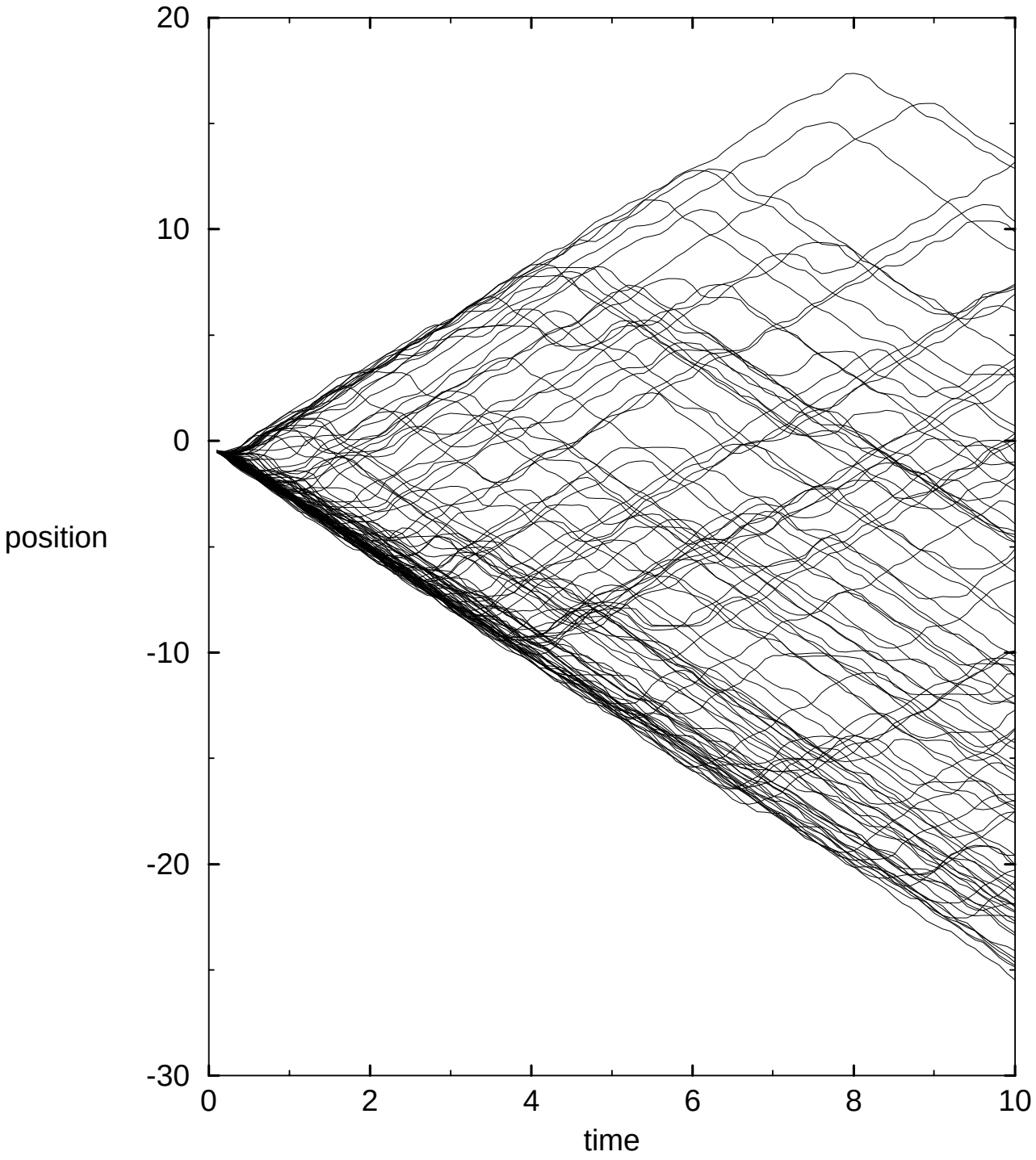

Figure 4.16: Position versus time for $N = 100$ with negative initial direction and $\Delta = 0.6$.

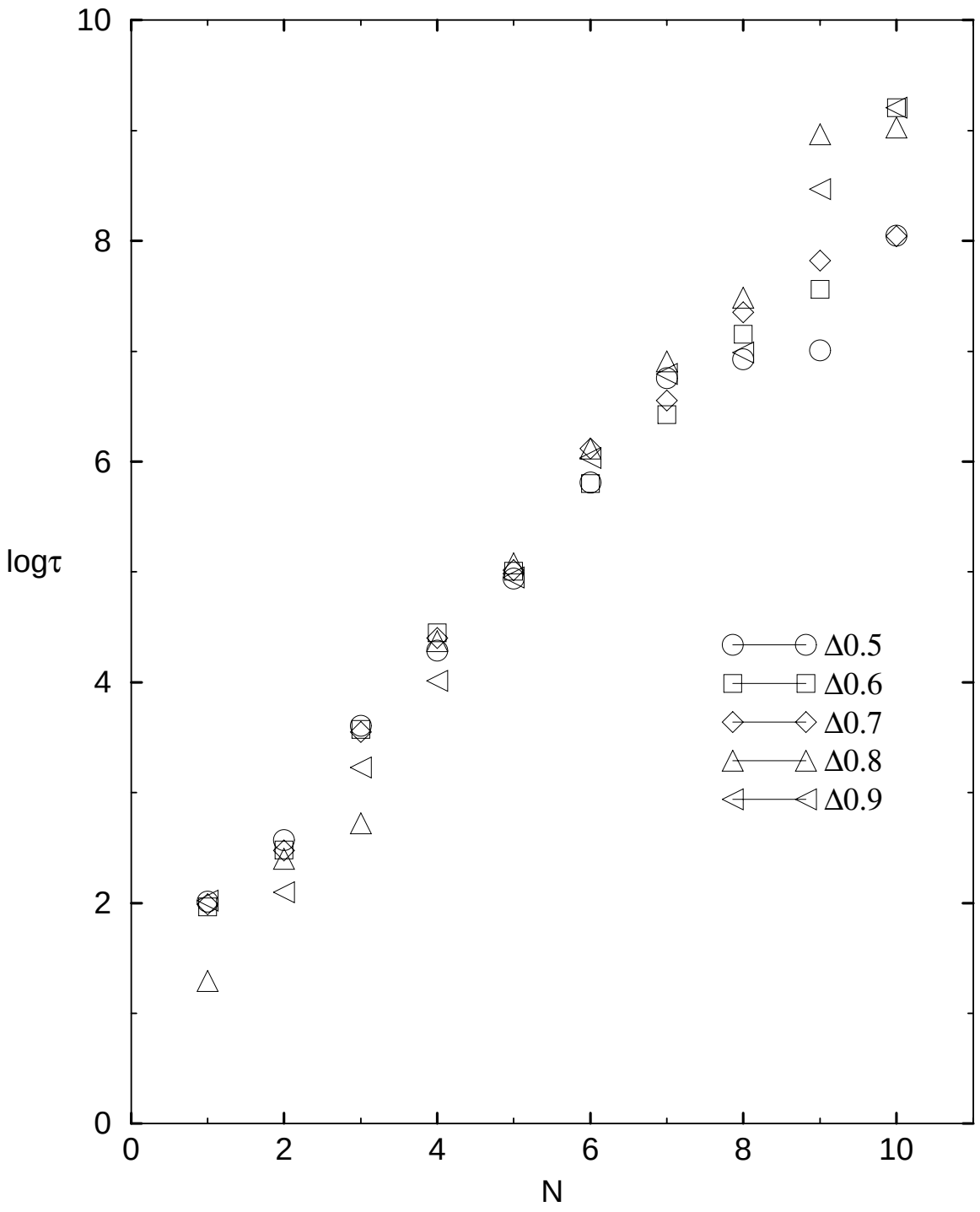

Figure 4.17: log τ versus N for different Δ values.

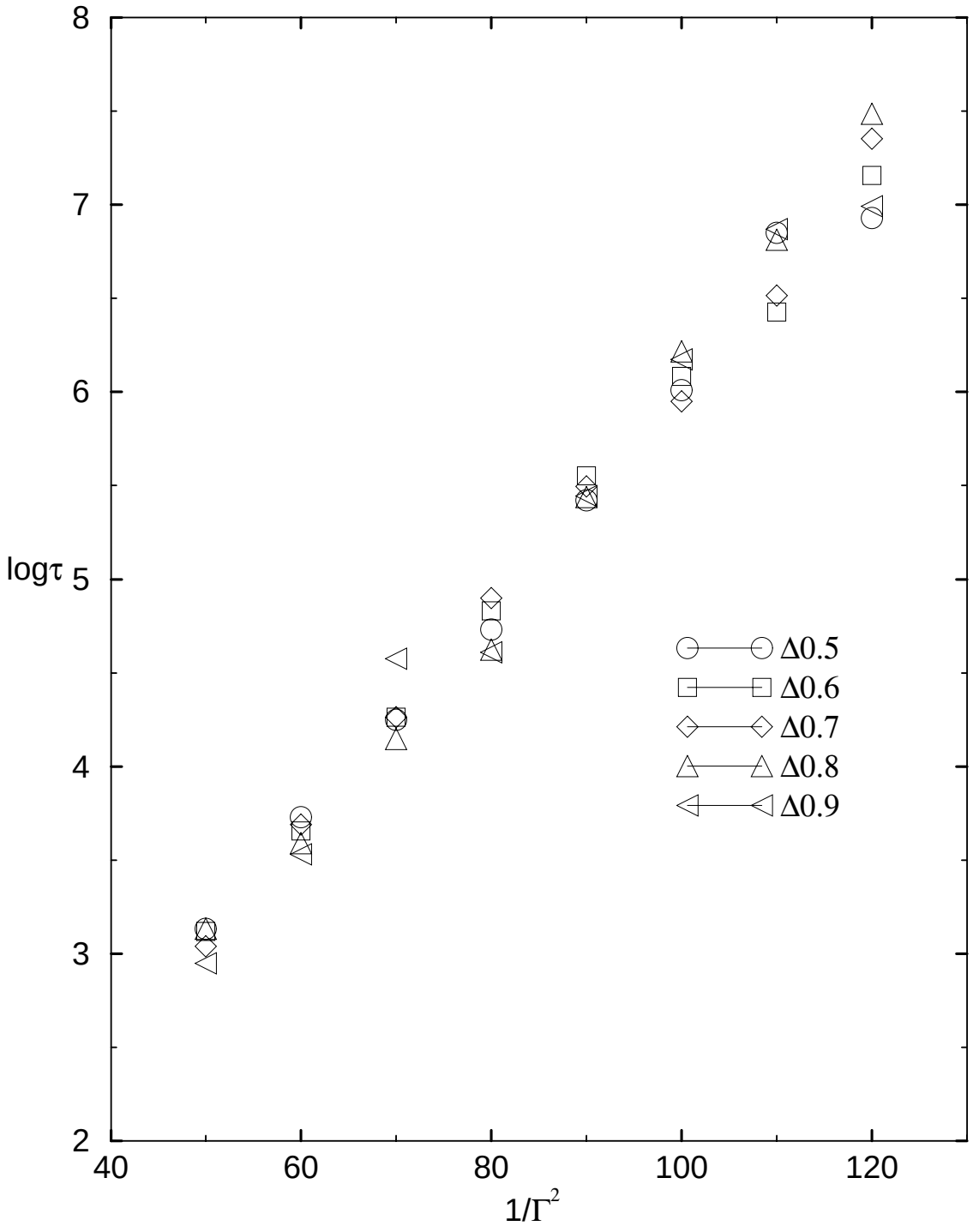

Figure 4.18: $\log \tau$ versus $1/\Gamma^2$ for different values Δ values and $N = 8$.

Chapter 5

CONCLUSION

In this thesis, we have investigated various aspects of cooperative molecular motor action. Deformation aspect considers the particle-particle interaction via inclusion of elastic forces into the standard model. Finite-size effect on the other hand involves finite chain length. Over-damped as well as under-damped systems, in the presence of symmetric and asymmetric ratchet potentials is investigated separately for this effect. One should emphasize that the standard model considers solutions for the infinite chain length limit, without particle-particle interactions. Therefore, our work is an extension of the work in this area which typically models the muscle contraction phenomena. We hope that this work serves for further experimental research in the area.

For the deformation of the cooperative molecular motors, the most remarkable phenomena is the change in the behavior of the force versus motor velocity dependence that is contributed by this effect. For large values of spring constant used in the model, the motor force increases. However, further increase in the spring constant results in abrupt drop in the motor force. There is a certain value of spring constant when the critical value of the friction constant reaches a maximum value for the motor operation. The three peak structure in the

population versus spatial coordinate graph for certain inter-particle distances is also interesting and was first displayed in our work. We conclude that deformation brings a richer structure and may yield a better motor for some range of parameters.

For the finite size effects in cooperative molecular motors, again there are two remarkable phenomena: 1. The intermittent switching behavior for the time dependence of velocity, and 2. the stalling of the motor system for small number of particles. We have analyzed the relationship between the intermittent velocity switching and the chain size by associating a time constant to this phenomenon. Noise is also used as an ingredient for further investigation.

The most striking feature of the finite size analysis is the fact that its effects are visible even in quite large ($N = 100$) systems.

Bibliography

[1] Force and Motion Generation of Molecular Motors: A Generic Description, F. Jülicher in Transport and Structure: Their Competitive Roles Biophysics and Chemistry Edited by S.C.Müller, J. Parisi, W.Zimmermann, Lect .Notes Physics (Springer 1999).

[2] S.Taneri and M.Cemal Yalabık,Eur.Phys. J.B22,403-407 (2001).

[3] Finite Size Effects in Cooperative Molecular Motors,S.Taneri and M. Cemal Yalabık(submitted to Physica A).

[4] F.Jülicher and J.Prost,Phys.Rev.Lett. 78,4510(1997).

[5] A.Vilfan,E.Frey,F. Schwabl,Eur.Phys J.B 3,535 (1998).

[6] A.Vilfan, E.Frey,F.Schwabl, Europhys. Lett.45,283 (1999).

[7] Imre Derényi and Tamas Viscek,Phys. Rev. Lett. 75,374 (1995).

[8] Jacob N. Israelachvili, Intermolecular Surface Forces, (1991).

[9] F.Jülicher and J.Prost,PhysRev. Lett. 75,2618 (1995).

[10] J.Prost,J.F.Chauwin,L.Peliti,A.Ajdari,Phys Rev. Lett.72,2652(1994) .

[11] S.Camalet and F.Julicher,New J. Phys.2,24(2000),physics/0003101 (30 March 2000).

[12] M.E. Fisher and A.B. Kolomeisky, Physica A 274,241 (1999).

[13] H.Risken,the Fokker-Plank Equation.56,3917, Springer Verlag, Ulm (1988).